ESAIM: M2AN 58 (2024) 1725–1754
https://doi.org/10.1051/m2an/2024023

ESAIM: Mathematical Modelling and Numerical Analysis
www.esaim-m2an.org

AN ULTRAWEAK-LOCAL DISCONTINUOUS GALERKIN METHOD FOR NONLINEAR BIHARMONIC SCHRÖDINGER EQUATIONS

Qi Wang[1] and Lu Zhang[2,3,*]

Abstract. This paper proposes and analyzes a fully discrete scheme for nonlinear biharmonic Schrödinger equations. We first write the single equation into a system of problems with second-order spatial derivatives and then discretize the space variable with an ultraweak discontinuous Galerkin scheme and the time variable with the Crank–Nicolson method. The proposed scheme proves to be computationally more efficient compared to the local discontinuous Galerkin method in terms of the number of equations needed to be solved at each single time step, and it is unconditionally stable without imposing any penalty terms. It also achieves optimal error convergence in L^2 norm both in the solution and in the auxiliary variable with general nonlinear terms. We also prove several physically relevant properties of the discrete schemes, such as the conservation of mass and the Hamiltonian for the nonlinear biharmonic Schrödinger equations. Several numerical studies demonstrate and support our theoretical results.

Mathematics Subject Classification. 65M12, 65M60.

Received May 25, 2023. Accepted April 3, 2024.

1. Introduction

Discontinuous Galerkin (DG) methods are a class of finite element methods that use completely discontinuous basis functions for both numerical solutions and test functions in spatial variables. Since their proposal in 1973 by Reed and Hill [34] for hyperbolic equations, and in 70's for elliptic equations (see, *e.g.*, [4–6, 39]), they have become very popular in solving PDEs. Moreover, due to their attractive properties such as arbitrary high-order accuracy, extremely local data structure, and *hp*-adaptivity, they have been widely used to solve problems in many areas of science, engineering, and industry. For details of the applications, we refer to [20, 24] and the references therein.

Over the past few decades, DGs methods have evolved in several directions. For example, Cockburn and Shu [19] propose the so-called local DG method to solve a large class of nonlinear convection-diffusion equations with high-order spatial derivatives. By introducing auxiliary variables that reduce the original problem to a lower-order system, typically with first-order spatial derivatives, local DG methods ensure the stability of the scheme through appropriate numerical fluxes embedded in the resulting system. See [26, 41, 42] and references

Keywords and phrases. Discontinuous Galerkin, nonlinear biharmonic Schrödinger equation, stability and error estimates.

[1] Southwestern University of Finance and Economics, 555 Liutai Ave, Wenjiang, Chengdu, Sichuan 611130, P.R. China.

[2] Department of Computational Applied Mathematics and Operations Research, Rice University, Houston, TX 77005, USA.

[3] Ken Kennedy Institute, Rice University, Houston, TX 77005, USA.

*Corresponding author: lz82@rice.edu

© The authors. Published by EDP Sciences, SMAI 2024

This is an Open Access article distributed under the terms of the Creative Commons Attribution License (https://creativecommons.org/licenses/by/4.0), which permits unrestricted use, distribution, and reproduction in any medium, provided the original work is properly cited.

therein for recent developments of the local DG method. Another stream of development is motivated by the urge to solve higher-order problems, and this includes the ultraweak DG introduced by Despres [25] for linear elliptic PDEs. The idea of the ultraweak DG method is to shift all spatial derivatives *via* integration by parts to the test function in the weak formulation, and the stability of the scheme is guaranteed by certain numerical fluxes and, if necessary, additional internal penalty terms. See [13, 14, 17, 36] and the references therein for the applications and further development of the ultraweak DG method.

1.1. Biharmonic Schrödinger equations and their numerical studies

Nonlinear biharmonic Schrödinger equations arise frequently from the study of propagations in intense laser beams, quantum mechanics, nonlinear optical fibers, electromagnetic beams in plasma, etc. See [1, 22, 30, 33] and references therein. In this paper, we consider nonlinear biharmonic Schrödinger equations of the following form

$$iu_t + \kappa\Delta^2 u + uF'(|u|^2) = 0, \quad (\mathbf{x}, t) \in \Omega \times (0, T], \quad \Omega \subseteq \mathbb{R}^d, \quad d = 1, 2, \tag{1.1}$$

where $u(\mathbf{x}, t)$ is a complex function of the space-time variable $(\mathbf{x}, t)$, where $|u|$ is its Euclidean length, $i = \sqrt{-1}$ is the imaginary number, $\Delta^2 = \big(\sum_{j=1}^d \frac{\partial^2}{\partial x_j^2}\big)^2$ is the biharmonic operator, $F'(y) = \frac{\mathrm{d}F}{\mathrm{d}y}$ is a real function measuring the medium nonlinearity, and κ is a real constant depending on the physical relevance. Problem (1.1) is a special form of the following equation with $\varepsilon = 0$

$$iu_t + \varepsilon\Delta u + \kappa\Delta^2 u + uF'(|u|^2) = 0, \tag{1.2}$$

which was introduced in [29, 30] to study the role of small fourth-order dispersion in the propagation of intense laser beams in a bulk medium.

For $F'(|u|^2) = |u|^{2\sigma}$, σ being a positive integer, the well-posedness and the formation of singularities for both (1.1) and (1.2) have been studied by many researchers over the past few decades. For example, Karpman [29], Karpman and Shagalov [30] have shown that the waveguide solutions of (1.2) are stable for all $\kappa < 0$ when $d\sigma \leq 2$ and for all $\kappa \ll -1$ when $2 < d\sigma < 4$, but these solutions are unstable for all $\kappa < 0$ when $\sigma d \geq 4$. These results carry over to the fourth order equation (1.1) according to [9, 27]. They prove that (1.1) is defocusing for $\kappa > 0$ and its solution exists globally, and it is focusing for $\kappa < 0$ and there exists a critical exponent $d\sigma = 4$ which determines the blow-ups and global existence subject to the (L^2) size of the initial data.

Before proceeding further, we want to note that several numerical methods have been proposed in the literature to solve nonlinear Schrödinger equations (1.2) for $\kappa = 0$, such as the finite difference methods [2, 7, 12, 15], the time-splitting pseudospectral methods [8, 32, 35], the finite element methods [3, 23, 28], and the DG methods [16, 41, 46]. However, only a few works have considered the problem for $\kappa \neq 0$. For example, Xiao *et al.* [40] propose a conservative linearly-implicit finite difference scheme for the modified Zakharov system that describes the coupling of high-frequency Langmuir waves (*e.g.*, biharmonic Schrödinger equation) and low-frequency ion-acoustic waves (*e.g.*, wave equations). The linearly-implicit finite difference method generates independent linear algebraic equations to be solved, and it has second-order convergence in space. Zhang and Su [45] improve the convergence of the method to the fourth order in space by developing a linearly implicit compact finite difference scheme. Note that both schemes are studied only in the one-dimensional case. On the other hand, Schrödinger equations in multiple dimensions have further applications, such as optimal observation or sensor location problems in piezoelectric actuators and damage detection. Baruch *et al.* [10, 11] investigate singular and ring type singular solutions of (1.1) in multidimensions by adaptive lattice methods and static lattice redistribution methods, respectively. No numerical analysis is conducted therein on the numerical methods concerning their stability, convergence, etc. Nevertheless, we want to emphasize that nonlinear Schrödinger equations with the higher-order dispersive term (1.2) in both one-dimensional and multi-dimensional cases not only play an important role in the physical model description, such as the quantum effect in the propagation of Langmuir waves in plasma but also bring interesting mathematical effects, such as the stabilization of soliton instabilities. Therefore, it is both theoretically and practically rewarding to develop stable and efficient numerical methods for a better understanding of the dynamics within nonlinear biharmonic Schrödinger equations.

1.2. Main results

This paper presents and analyzes a fully discrete ultraweak-local DG scheme with the Crank–Nicolson time discretization for the nonlinear biharmonic Schrödinger equation (1.1). The proposed scheme is implicit in time, unconditionally stable, and preserves the mass and Hamiltonian associated with the problem at the fully discrete level. We are motivated by Tao *et al.* [37, 38] and Zhang [44] to introduce a second-order spatial derivative as an auxiliary variable to reduce the fourth-order problem to a second-order system in space. This allows us to ensure the stability of the proposed scheme through the integration by parts and a suitable choice of numerical fluxes. In particular, its stability can be achieved without the need for internal penalty terms compared to the ultraweak DG method, which also improves the robustness of this new scheme. This hybrid approach requires only one auxiliary variable regardless of the dimension of the problem and greatly reduces the memory and computational cost of the local DG method, see Remark 1 for detailed discussion.

The rest of the paper is organized as follows. In Section 2, we first present the governing equations and their DG formulation. Then, we study and discuss the stability of our proposed scheme formulated in Theorem 1. Section 3 introduces some projection operators and presents in Theorem 2 the optimal L^2 error estimates for the semi-discrete scheme through an auxiliary equation and suitable numerical fluxes. Section 4 then presents the fully discrete ultraweak-local DG coupled to the Crank–Nicolson time discretization and proves its mass and Hamiltonian conserving properties in Theorem 3. Some numerical experiments in both 1D and 2D which demonstrate and verify the theoretical results are presented in Section 5. A summary of this work is given in Section 6.

2. Semi-discrete DG formulation and stability

We choose $\kappa = 1$ in (1.1) and consider the following nonlinear biharmonic Schrödinger equation over a bounded domain $\Omega \subseteq \mathbb{R}^d$, $d \geq 1$, with a piecewise smooth boundary $\partial\Omega$

$$iu_t + \Delta^2 u = -uF'(|u|^2), \quad \mathbf{x} \in \Omega \subseteq \mathbb{R}^d, \quad t \geq 0, \tag{2.1}$$

under an initial condition and periodic boundary condition. Note that $\kappa = 1$ is chosen for ease of demonstration, and the proposed method applies to cases where κ takes other values; moreover, our scheme cooperates with more general boundary conditions and we restrict our analysis to periodic boundary conditions to simplicity the discussion, but present numerical studies with general boundary conditions in Section 5.1. We also assume that $F(|u|^2) \geq 0$ so that (2.1) has a strictly positive Hamiltonian; when $F(|u|^2) < 0$, the problem (2.1) is said to be focusing, where control of the H^2 norm with the Hamiltonian is no longer possible.

To derive a DG formulation for (2.1), we denote $w := \Delta u$ and write it into

$$\begin{cases} iu_t = -\Delta w - uF'(|u|^2), \\ w = \Delta u. \end{cases} \tag{2.2}$$

Note that any solution to (2.2) formally satisfies the conservation of mass and the Hamiltonian

$$M(t) = M(0), \quad H(t) = H(0) \qquad \forall t > 0,$$

where the mass and the Hamiltonian are given by

$$M(t) := \int_\Omega |u|^2 \, \mathrm{d}\mathbf{x}, \quad \text{and} \quad H(t) := \int_\Omega |w|^2 + F(|u|^2) \, \mathrm{d}\mathbf{x}.$$

2.1. Notations

We will now introduce the notations used for our numerical analysis. Let the spatial domain be $\Omega = \Pi_{j=1}^d [x_j^a, x_j^b]$ with a Cartesian mesh

$$\Omega_h = \left\{ K \;\middle|\; K = \Pi_{j=1}^d I_{kx_j}, 1 \leq kx_j \leq N_{x_j} \right\},$$

where $I_{kx_j} = [x_{j,kx_j-\frac{1}{2}}, x_{j,kx_j+\frac{1}{2}}]$ is a subinterval in the partition of $\left[x_j^a, x_j^b\right] : x_j^a = x_{j,\frac{1}{2}} < x_{j,\frac{3}{2}} < \cdots < x_{j,N_{x_j}+\frac{1}{2}} = x_j^b$. For each element K we denote its length in x_j-direction as $x_{j,kx_j+\frac{1}{2}} - x_{j,kx_j-\frac{1}{2}}$. We further write $h = \max_{K\in\Omega_h}(x_{j,kx_j+\frac{1}{2}} - x_{j,kx_j-\frac{1}{2}})$ and use $\mathcal{F}_h$ to denote the collection of inter-element faces of Ω_h. Further, the mesh is quasi-uniform such that $h \le \delta(x_{j,kx_j+\frac{1}{2}} - x_{j,kx_j-\frac{1}{2}})$ for some positive constant δ. Then, on each element K we approximate the duo (u, w) by its discrete counterparts (u_h, w_h), each component belonging to the space of piecewise polynomials of degree defined by

$$V_h^q := \{v_h(\mathbf{x}) \big| v_h(\mathbf{x}) \in \mathcal{Q}^q(K), \mathbf{x} \in K \quad \forall K \in \Omega_h\},$$

where $\mathcal{Q}^q(K)$ is the space of tensor products of polynomials of degree at most q in each variable x_j defined on K. Specifically, if we denote $x_1 = x$ and $x_2 = y$, then

$$\Omega_h := \begin{cases} \cup_{j=1}^N \left[x_{j-\frac{1}{2}}, x_{j+\frac{1}{2}}\right] & \text{in 1D,} \\ \cup_{kj} \left[x_{k-\frac{1}{2}}, x_{k+\frac{1}{2}}\right] \times \left[y_{j-\frac{1}{2}}, y_{j+\frac{1}{2}}\right], \quad k = 1, \cdots, N_x, \quad j = 1, \cdots, N_y & \text{in 2D,} \end{cases}$$

and

$$K := \begin{cases} I_j = \left(x_{j-\frac{1}{2}}, x_{j+\frac{1}{2}}\right), & j = 1, 2, \cdots, N \qquad \text{in 1D,} \\ I_k \times I_j = \left(x_{k-\frac{1}{2}}, x_{k+\frac{1}{2}}\right) \times \left(y_{j-\frac{1}{2}}, y_{j+\frac{1}{2}}\right), & k = 1, \cdots, N_x, \quad j = 1, \cdots, N_y \qquad \text{in 2D.} \end{cases}$$

In 1D, for any $\eta \in V_h^q$, we denote η^- and η^+ to be the right and left limit values of η at $x_{j+\frac{1}{2}}$, respectively. Let $\mathbf{n}_\mathrm{L} = -1$ and $\mathbf{n}_\mathrm{R} = 1$ be the outward unit normal to the left and right end of each sub-cell I_j, respectively, we then have the average and the jump at $x_{j+\frac{1}{2}}$ as follows

$$\{\eta\}_{j+\frac{1}{2}} := \frac{1}{2}\left(v^+_{j+\frac{1}{2}} + v^-_{j+\frac{1}{2}}\right), \quad [\eta]_{j+\frac{1}{2}} := v^-_{j+\frac{1}{2}}\mathbf{n}_\mathrm{L} + v^+_{j+\frac{1}{2}}\mathbf{n}_\mathrm{R}.$$

In 2D, let e be an interior edge shared by the "left" and "right" elements denoted by K_L and K_R. The "left" and "right" can be uniquely defined for each e according to any fixed rule. In this work, considering the rectangle for Cartesian meshes, we refer to the left and bottom directions as "left" and the right and top directions as "right". Let ζ be a continuously differentiable scalar function on K_L and K_R, and $\zeta^- := (\zeta|_{K_\mathrm{L}})|_e$, $\zeta^+ := (\zeta|_{K_\mathrm{R}})|_e$ be the left and right traces, respectively. We then introduce the conventional notations for averages and jumps of scalar-valued function ζ and vector-valued function $\boldsymbol{\zeta}$ as follows

$$\{\zeta\} := \frac{1}{2}(\zeta^- + \zeta^+),\ [\zeta] := \zeta^-\mathbf{n}_\mathrm{L} + \zeta^+\mathbf{n}_\mathrm{R},\ \{\boldsymbol{\zeta}\} := \frac{1}{2}(\boldsymbol{\zeta}^- + \boldsymbol{\zeta}^+),\ [\boldsymbol{\zeta}] := \boldsymbol{\zeta}^- \cdot \mathbf{n}_\mathrm{L} + \boldsymbol{\zeta}^+ \cdot \mathbf{n}_\mathrm{R},$$

where $\mathbf{n}_\mathrm{L}$ and $\mathbf{n}_\mathrm{R}$ are the outward unit normals to ∂K_L and ∂K_R, respectively.

2.2. Semi-discrete DG formulation

To find an approximation of the second-order system, on each element $K \in \Omega_h$ we test the first and the second equation in (2.2) by functions $\phi, \psi \in V_h^q$. Integration by parts gives rise to

$$\int_K iu_{ht}\phi + w_h\Delta\phi + u_h F'\left(|u_h|^2\right)\phi \,\mathrm{d}\mathbf{x} = \int_{\partial K} -\widetilde{\nabla w_h} \cdot \mathbf{n}\phi + \widetilde{w_h}\nabla\phi \cdot \mathbf{n} \,\mathrm{d}S \tag{2.3}$$

and

$$\int_K w_h\psi - u_h\Delta\psi \,\mathrm{d}\mathbf{x} = \int_{\partial K} \widehat{\nabla u_h} \cdot \mathbf{n}\psi - \widehat{u_h}\nabla\psi \cdot \mathbf{n} \,\mathrm{d}S, \tag{2.4}$$

where $\widetilde{\nabla w_h}$, $\widetilde{w_h}$, $\widehat{\nabla u_h}$, and $\widehat{u_h}$ are numerical fluxes at element boundaries, and $\mathbf{n}$ is the outward unit normal to ∂K.

To complete the DG formulation, we specify the numerical fluxes $\widetilde{\nabla w_h}$, $\widetilde{w_h}$, $\widehat{\nabla u_h}$ and $\widehat{u_h}$ at the element boundaries by choosing

$$\widehat{u_h} = \alpha_1 u_h^+ + (1-\alpha_1)u_h^-,\ \widetilde{\nabla w_h} = (1-\alpha_1)\nabla w_h^+ + \alpha_1 \nabla w_h^-, \tag{2.5}$$

and

$$\widehat{\nabla u_h} = \alpha_2 \nabla u_h^+ + (1-\alpha_2)\nabla u_h^-,\ \widetilde{w_h} = (1-\alpha_2) w_h^+ + \alpha_2 w_h^-, \tag{2.6}$$

where $\alpha_1, \alpha_2 \in \mathbb{R}$. In particular, when $(\alpha_1, \alpha_2) = (0,1)$ or $(1,0)$, we have the alternating fluxes compatible with the error estimates in Sections 3.3 and 3.4.

For the simplicity of presentation, we denote

$$\mathcal{B}_K^1(w_h, \phi) := \int_K w_h \Delta\phi \,\mathrm{d}\mathbf{x} + \int_{\partial K} \widetilde{\nabla w_h}\cdot\mathbf{n}\phi - \widetilde{w_h}\nabla\phi\cdot\mathbf{n}\,\mathrm{d}S, \tag{2.7}$$

$$\mathcal{B}_K^2(u_h, \psi) := \int_K -u_h \Delta\psi \,\mathrm{d}\mathbf{x} - \int_{\partial K} \widehat{\nabla u_h}\cdot\mathbf{n}\psi - \widehat{u_h}\nabla\psi\cdot\mathbf{n}\,\mathrm{d}S. \tag{2.8}$$

Then one can further simplify (2.3) and (2.4) into

$$\int_K i u_{ht}\phi + u_h F'\big(|u_h|^2\big)\phi \,\mathrm{d}\mathbf{x} + \mathcal{B}_K^1(w_h, \phi) = 0, \tag{2.9}$$

and

$$\int_K w_h \psi \,\mathrm{d}\mathbf{x} + \mathcal{B}_K^2(u_h, \psi) = 0. \tag{2.10}$$

Remark 1. The local DG method requires $2d+1$ auxiliary variables to transform the original fourth-order problem into a first-order system in space, while our proposed scheme requires only one additional variable, regardless of the dimension d of the problem. Accordingly, at each time step our method only needs to evaluate 9 integrals in (2.9) and (2.10), and this is more economical compared to the local DG method, which needs to evaluate $6d+7$ integrals (*cf.* [26]).

2.3. Energy conservation

We now prove that the proposed scheme formulated in (2.9) and (2.10) preserves both the semi-discrete mass and the semi-discrete Hamiltonian. In particular, we show that they imply the stability of the scheme as follows.

Theorem 1. *The solution of the DG scheme* (2.9) *and* (2.10) *with numerical fluxes* (2.5) *and* (2.6) *satisfies the following conservation laws for all* $t > 0$

$$M_h(t) = \int_{\Omega_h} |u_h|^2 \,\mathrm{d}\mathbf{x} = M_h(0), \tag{2.11}$$

$$H_h(t) = \int_{\Omega_h} |w_h|^2 + F(|u_h|^2)\,\mathrm{d}\mathbf{x} = H_h(0). \tag{2.12}$$

Proof. We first prove the conservation of mass. Multiply (2.9) by $-i$, (2.10) by i, choose $\phi = u_h^*$ in (2.9) and $\psi = w_h^*$ in (2.10), where "$*$" denotes the complex conjugate, and then sum them up over all elements K. We get that

$$-i\sum_K \mathcal{B}_K^1(w_h, u_h^*) - i\int_{\Omega_h} i u_{ht} u_h^* + |u_h|^2 F'\big(|u_h|^2\big)\,\mathrm{d}\mathbf{x} = 0, \tag{2.13}$$

and

$$i\sum_K \mathcal{B}_K^2(u_h, w_h^*) + \int_{\Omega_h} i w_h w_h^* \,\mathrm{d}\mathbf{x} = 0, \tag{2.14}$$

where $\mathcal{B}_K^1$ and $\mathcal{B}_K^2$ are defined in (2.7) and (2.8), respectively. Let $\mathcal{F}_h$ be the interelement boundary face shared by two neighboring elements (*e.g.*, $\mathcal{F}_h$ are the two points on the boundary in 1D and the interior edges in 2D). Thanks to the periodic boundary condition, we integrate by parts to collect

$$-i\sum_K \mathcal{B}_K^1(w_h,u_h^*) = \int_{\Omega_h} i\nabla w_h\cdot\nabla u_h^*\,\mathrm{d}\mathbf{x} - i\sum_F\int_F \widetilde{\nabla w_h}\cdot[u_h^*] - \widetilde{w_h}[\nabla u_h^*] + [w_h\nabla u_h^*]\,\mathrm{d}S, \tag{2.15}$$

and

$$i\sum_K \mathcal{B}_K^2(u_h,w_h^*) = \int_{\Omega_h} i\nabla u_h\cdot\nabla w_h^*\,\mathrm{d}\mathbf{x} - i\sum_F\int_F \widehat{\nabla u_h}\cdot[w_h^*] - \widehat{u_h}[\nabla w_h^*] + [u_h\nabla w_h^*]\,\mathrm{d}S. \tag{2.16}$$

Then, substituting (2.15) and (2.16) into (2.13) and (2.14), respectively, computing the complex conjugate of the resulting two equations and adding them together with (2.13) and (2.14), we arrive at

$$\begin{aligned}
0 &= i\int_{\Omega_h}|u_h|^2F'\big(|u_h|^2\big)\,\mathrm{d}\mathbf{x} - i\int_{\Omega_h}|u_h|^2F'(|u_h|^2)\,\mathrm{d}\mathbf{x}\\
&= \frac{\mathrm{d}}{\mathrm{d}t}\int_{\Omega_h}|u_h|^2\mathrm{d}\mathbf{x} - i\sum_K \mathcal{B}_K^1(w_h,u_h^*) - \mathcal{B}_K^1(w_h^*,u_h) - \mathcal{B}_K^2(u_h,w_h^*) + \mathcal{B}_K^2(u_h^*,w_h)\\
&= \frac{\mathrm{d}}{\mathrm{d}t}\int_{\Omega_h}|u_h|^2\mathrm{d}\mathbf{x} + 2\mathrm{Im}\left(\sum_F\int_F \widetilde{\nabla w_h}\cdot[u_h^*] - \widetilde{w_h}[\nabla u_h^*] + [w_h\nabla u_h^*]\,\mathrm{d}S\right)\\
&\quad + 2\mathrm{Im}\left(\sum_F\int_F \widehat{\nabla u_h}\cdot[w_h^*] - \widehat{u_h}[\nabla w_h^*] + [u_h\nabla w_h^*]\,\mathrm{d}S\right).
\end{aligned} \tag{2.17}$$

Further, by using the fact

$$[ab] = \big((1-\theta)a^- + \theta a^+\big)[b] + \big((1-\theta)b^+ + \theta b^-\big)[a],\quad \theta\in[0,1], \tag{2.18}$$

we get

$$\begin{aligned}
\mathcal{K}_1 &:= \sum_F\int_F [w_h\nabla u_h^*] + \widehat{\nabla u_h}\cdot[w_h^*] - \widetilde{w_h}[\nabla u_h^*]\,\mathrm{d}S\\
&= \sum_F\int_F \big(\alpha_2 w_h^- + (1-\alpha_2)w_h^+\big)[\nabla u_h^*] + \big((1-\alpha_2)\nabla u_h^{*,-} + \alpha_2\nabla u_h^{*,+}\big)\cdot[w_h]\\
&\quad + \big(\alpha_2\nabla u_h^+ + (1-\alpha_2)\nabla u_h^-\big)\cdot[w_h^*] - \big((1-\alpha_2)w_h^+ + \alpha_2 w_h^-\big)[\nabla u_h^*]\,\mathrm{d}S\\
&= \sum_F\int_F 2\mathrm{Re}\big(\big((1-\alpha_2)\nabla u_h^- + \alpha_2\nabla u_h^+\big)\cdot[w_h^*]\big)\,\mathrm{d}S,
\end{aligned} \tag{2.19}$$

and

$$\begin{aligned}
\mathcal{K}_2 &:= \sum_F\int_F [u_h\nabla w_h^*] + \widetilde{\nabla w_h}\cdot[u_h^*] - \widehat{u_h}[\nabla w_h^*]\,\mathrm{d}S\\
&= \sum_F\int_F 2\mathrm{Re}\big(\big((1-\alpha_1)\nabla w_h^+ + \alpha_1\nabla w_h^-\big)\cdot[u_h^*]\big)\,\mathrm{d}S.
\end{aligned} \tag{2.20}$$

These identities indicate both $\mathcal{K}_1$ and $\mathcal{K}_2$ are real. Plugging (2.19) and (2.20) into (2.17) leads us to

$$\frac{\mathrm{d}}{\mathrm{d}t}\int_{\Omega_h}|u_h|^2\,\mathrm{d}\mathbf{x} = 0,$$

which yields the conservation of mass in (2.11).

To prove the conservation of Hamiltonian in (2.12), we differentiate (2.10) with respect to time

$$\int_K w_{ht}\psi \,\mathrm{d}\mathbf{x} + \mathcal{B}_K^2(u_{ht},\psi) = 0, \tag{2.21}$$

where $\mathcal{B}_K^2$ is defined in (2.8). Now, by choosing $\phi = u_{ht}^*$ in (2.9), $\psi = w_h^*$ in (2.21) and summing them over all elements K, respectively, we get

$$\sum_K \mathcal{B}_K^1(w_h, u_{ht}^*) + \int_{\Omega_h} iu_{ht}u_{ht}^* + u_h F'(|u_h|^2)u_{ht}^* \,\mathrm{d}\mathbf{x} = 0 \tag{2.22}$$

and

$$\sum_K \mathcal{B}_K^2(u_{ht}, w_h^*) + \int_{\Omega_h} w_{ht}w_h^* \,\mathrm{d}\mathbf{x} = 0, \tag{2.23}$$

where $\mathcal{B}_K^1$ is defined in (2.7). Moreover, we integrate by parts and have

$$\sum_K \mathcal{B}_K^1(w_h, u_{ht}^*) = \int_{\Omega_h} -\nabla w_h \cdot \nabla u_{ht}^* \,\mathrm{d}\mathbf{x} + \sum_F \int_F \widetilde{\nabla w_h} \cdot [u_{ht}^*] - \widetilde{w_h}[\nabla u_{ht}^*] + [w_h \nabla u_{ht}^*] \,\mathrm{d}S,$$

and

$$\sum_K \mathcal{B}_K^2(u_{ht}, w_h^*) = \int_{\Omega_h} \nabla u_{ht} \cdot \nabla w_h^* \,\mathrm{d}\mathbf{x} - \sum_F \int_F \widehat{\nabla u_{ht}} \cdot [w_h^*] - \widehat{u_{ht}}[\nabla w_h^*] + [u_{ht}\nabla w_h^*] \,\mathrm{d}S.$$

Then, summing the complex conjugates of (2.22) and (2.23) up yields

$$\begin{aligned}
\frac{\mathrm{d}}{\mathrm{d}t}\int_{\Omega_h} F(|u_h|^2) + |w_h|^2 \,\mathrm{d}\mathbf{x} &= -\sum_K \mathcal{B}_K^1(w_h, u_{ht}^*) + \mathcal{B}_K^1(w_h^*, u_{ht}) + \mathcal{B}_K^2(u_{ht}, w_h^*) + \mathcal{B}_K^2(u_{ht}^*, w_h) \\
&= -2\mathrm{Re}\left(\sum_F \int_F \widetilde{\nabla w_h} \cdot [u_{ht}^*] - \widetilde{w_h}[\nabla u_{ht}^*] + [w_h \nabla u_{ht}^*] \,\mathrm{d}S\right) \\
&\quad + 2\mathrm{Re}\left(\sum_F \int_F \widehat{\nabla u_{ht}} \cdot [w_h^*] - \widehat{u_{ht}}[\nabla w_h^*] + [u_{ht}\nabla w_h^*] \,\mathrm{d}S\right).
\end{aligned} \tag{2.24}$$

Using identity (2.18) and the numerical fluxes (2.5) and (2.6), we have

$$\begin{aligned}
\mathcal{K}_3 &:= \sum_F \int_F [w_h \nabla u_{ht}^*] - \widetilde{w_h}[\nabla u_{ht}^*] - \widehat{\nabla u_{ht}} \cdot [w_h^*] \,\mathrm{d}S \\
&= -2i \sum_F \int_F \mathrm{Im}\big(\big((1-\alpha_2)\nabla u_{ht}^- + \alpha_2 \nabla u_{ht}^+\big) \cdot [w_h^*]\big) \,\mathrm{d}S,
\end{aligned} \tag{2.25}$$

and

$$\begin{aligned}
K_4 &:= \sum_F \int_F -[u_{ht}\nabla w_h^*] + \widetilde{\nabla w_h} \cdot [u_{ht}^*] + \widehat{u_{ht}}[\nabla w_h^*] \,\mathrm{d}S \\
&= 2i \sum_F \int_F \mathrm{Im}\Big(\big((1-\alpha_1)\nabla w_h^+ + \alpha_1 \nabla w_h^-\big) \cdot [u_{ht}^*]\Big) \,\mathrm{d}S.
\end{aligned} \tag{2.26}$$

Again, these identities indicate both $\mathcal{K}_3$ and $\mathcal{K}_4$ are purely imaginary. Finally, substituting (2.25) and (2.26) into (2.24) leads us to

$$\frac{\mathrm{d}}{\mathrm{d}t}\int_{\Omega_h} F(|u_h|^2) + |w_h|^2 \,\mathrm{d}\mathbf{x} = 0,$$

and this proves the conservation of Hamiltonian in (2.12). □

Remark 2. To extend (2.5) and (2.6), we can consider the following general form of numerical fluxes:

$$\begin{aligned}
\widehat{u_h} &:= \alpha_1 u_h^+ + (1-\alpha_1)u_h^- + \beta_1\big(\nabla w_h^+\mathbf{n}^+ + \nabla w_h^-\mathbf{n}^-\big) + \boldsymbol{\theta}_1\cdot(u_h^-\mathbf{n}^- + u_h^+\mathbf{n}^+),\\
\widetilde{w_h} &:= (1-\alpha_2)w_h^+ + \alpha_2 w_h^- - \tau_2\big(\nabla u^+\cdot\mathbf{n}^+ + \nabla u^-\cdot\mathbf{n}^-\big) + \boldsymbol{\theta}_2\cdot(w_h^+\mathbf{n}^+ + w_h^-\mathbf{n}^-),\\
\widetilde{\nabla u_h} &:= \alpha_2\nabla u_h^+ + (1-\alpha_2)\nabla u_h^- - \beta_2\big(w_h^+\mathbf{n}^+ + w_h^-\mathbf{n}^-\big) - \boldsymbol{\theta}_2(\nabla u_h^+\cdot\mathbf{n}^+ + \nabla u_h^-\cdot\mathbf{n}^-),\\
\widetilde{\nabla w_h} &:= (1-\alpha_1)\nabla w_h^+ + \alpha_1\nabla w_h^- + \tau_1\big(u_h^+\mathbf{n}^+ + u_h^-\mathbf{n}^-\big) - \boldsymbol{\theta}_1\big(\nabla w_h^+\cdot\mathbf{n}^+ + \nabla w_h^-\cdot\mathbf{n}^-\big),
\end{aligned}$$

where $\boldsymbol{\theta}_1 = \big(\theta_1^{(1)}, \theta_1^{(2)}\big), \boldsymbol{\theta}_2 = \big(\theta_2^{(1)}, \theta_2^{(2)}\big)$, and $\alpha_i, \theta_1^{(i)}, \theta_2^{(i)} \in \mathbb{R}$, and $\beta_i, \tau_i \geq 0$ are upwinding parameters, $i = 1, 2$. In particular, if β_i and τ_i are not all zeros, $i = 1, 2$, we have dissipating schemes.

3. Error estimates

In this section, we derive error estimates of the DG scheme (2.9) and (2.10) proposed for the nonlinear biharmonic Schrödinger equation (2.1). For simplicity of notation and without loss of generality, we consider only the following alternating fluxes with $\alpha_1 = \alpha_2 = 1$ in (2.5) and (2.6), *i.e.*,

$$\widehat{u_h} = u_h^+, \quad \widetilde{\nabla w_h} = \nabla w_h^-, \quad \widetilde{\nabla u_h} = \nabla u_h^+, \quad \widetilde{w_h} = w_h^-. \tag{3.1}$$

However, the error analysis can be easily generated for other types of alternating fluxes (*e.g.*, $(\alpha_1, \alpha_2) = (0, 0)$ or $(\alpha_1, \alpha_2) = (1, 0)$ or $(\alpha_1, \alpha_2) = (0, 1)$ in (2.5) and (2.6)). In Section 3.1, we review some projections and inequalities that are essential for our proof. Section 3.2 presents *a priori* error estimates needed to evaluate the nonlinear terms. The error estimates in the L^2 norm are given from Sections 3.3 and 3.4. In all that follows, we denote by C a generic positive constant that is independent of h but can vary from line to line.

3.1. Projections

We now introduce some projections used in the error estimates. For any $q \geq 1$, in 1D, we define the Gauss–Radau projections $P_h^\pm$ into V_h^q such that for any $u \in H^{q+1}(\Omega_h)$ and for any $q \geq 2$

$$\int_{I_j} (P_h^\pm u - u)v_h \,\mathrm{d}x = 0 \qquad \forall v_h \in \mathcal{P}^{q-2}(I_j),$$

$$P_h^+ u\Big(x_{j-\frac12}^+\Big) = u\Big(x_{j-\frac12}\Big), \quad (P_h^+ u)_x\Big(x_{j-\frac12}^+\Big) = u_x\Big(x_{j-\frac12}\Big), \tag{3.2}$$

$$P_h^- u\Big(x_{j+\frac12}^-\Big) = u\Big(x_{j+\frac12}\Big), \quad (P_h^- u)_x\Big(x_{j+\frac12}^-\Big) = u_x\Big(x_{j+\frac12}\Big). \tag{3.3}$$

Note that when $q = 1$, the Gauss–Radau projections are defined only by (3.2) and (3.3).

In 2D, we define the Gauss–Radau projections to be

$$\Pi_h^\pm u := \Big(P_{hx}^\pm \otimes P_{hy}^\pm\Big)u,$$

where the subscripts $x(y)$ indicate the application of the one-dimensional operators $P_h^\pm$ in the $x(y)$-direction. For the detailed formulation of $\Pi_h^\pm u$, we refer to [37].

In both 1D and 2D, the following inequality holds (see *e.g.*, [18,21]): for small enough h, there exists a positive constant C dependent of q but independent of h such that for any $u \in H^{q+1}(\Omega_h)$

$$\|u - Q_h u\|_{L^2(\Omega_h)} + h\|u - Q_h u\|_{L^\infty(\Omega_h)} + h^{\frac12}\|u - Q_h u\|_{L^2(\Gamma_h)} \leq C h^{q+1}, \tag{3.4}$$

where $Q_h = P_h^\pm$ in 1D and $Q_h = \Pi_h^\pm$ in 2D.

3.2. *A priori* error estimate

Let us denote

$$\begin{aligned} e_u &= u - u_h = u - \mathbb{P}_h^+ u + \mathbb{P}_h^+ u - u_h =: \eta_u + \xi_u, \\ e_w &= w - w_h = w - \mathbb{P}_h^- w + \mathbb{P}_h^- w - w_h =: \eta_w + \xi_w, \\ e_{ut} &= u_t - u_{ht} = u_t - \mathbb{P}_h^+ u_t + \mathbb{P}_h^+ u_t - u_{ht} =: \eta_{ut} + \xi_{ut}, \end{aligned}$$

where $\mathbb{P}_h^\pm = P_h^\pm$ when $d = 1$, and $\mathbb{P}_h^\pm = \Pi_h^\pm$ when $d = 2$. Note that [43] proves optimal convergence in L^2 norm for a second-order Schrödinger equation with polynomial nonlinearity without assuming *a prior* estimates for errors. However, for fourth-order nonlinear Schrödinger equations, especially those with strong nonlinearity as invested in this paper, following the lines of [21], for now we would like to make the following *a priori* assumption for some h small

$$\|e_u\|_{L^2(K)} + \|e_{ut}\|_{L^2(K)} \le h \qquad \forall 0 \le t \le T, \tag{3.5}$$

and by the interpolation property (3.4)

$$\|e_u\|_{L^\infty(K)} + \|e_{ut}\|_{L^\infty(K)} \le C \qquad \forall 0 \le t \le T. \tag{3.6}$$

These inequalities will be heavily used in establishing the error estimates. We will verify (3.5) in Section 3.5. In addition, to obtain an optimal error estimate in 2-D, we also need some superconvergence results regarding $\mathcal{B}_K^1$ and $\mathcal{B}_K^2$.

Lemma 1 ([37]). *Let $\mathcal{B}_K^1$ and $\mathcal{B}_K^2$ be defined by (2.7) and (2.8). We then have for $q \ge 1$,*

$$\begin{aligned} \left|\mathcal{B}_K^1(\eta_w, \phi)\right| &\le Ch^{q+2}\|w(\cdot,t)\|_{W^{2q+4,\infty}(K)}\|\phi\|_{L^2(K)}, \\ \left|\mathcal{B}_K^2(\eta_u, \psi)\right| &\le Ch^{q+2}\|u(\cdot,t)\|_{W^{2q+4,\infty}(K)}\|\psi\|_{L^2(K)}, \end{aligned}$$

where $\phi, \psi \in \mathcal{Q}^k(K)$, and the constant C is independent of h.

3.3. Error estimates for initial conditions

We now study the initial error estimates for the optimal error estimates of the DG scheme (2.9) and (2.10). Motivated by Li *et al.* [31] and Zhang *et al.* [46], we choose an initial approximation of a linear steady state given in the following lemma.

Lemma 2. *Suppose that $F \in C^{4,\zeta}(\mathbb{R})$ for some $\zeta \in (0,1)$, and u is sufficiently smooth, and the numerical initial condition of the DG scheme (2.9) and (2.10) is chosen as the DG approximation with numerical fluxes (3.1) to a linear steady-state problem*

$$iu + \Delta^2 u = iu_0 + \Delta^2 u_0, \tag{3.7}$$

where u_0 is the initial value of u, and periodic boundary conditions are considered. Further, denote $w = \Delta u$, then the DG approximation for (3.7) is given by

$$\int_K iu_h\phi + w_h\Delta\phi - \big(iu_0 + \Delta^2 u_0\big)\phi \,\mathrm{d}\mathbf{x} = \int_{\partial K} -\widetilde{\nabla w_h}\cdot\mathbf{n}\phi + \widetilde{w_h}\nabla\phi\cdot\mathbf{n}\,\mathrm{d}S, \tag{3.8}$$

and

$$\int_K w_h\psi - u_h\Delta\psi \,\mathrm{d}\mathbf{x}\,\mathrm{d}\mathbf{x} = \int_{\partial K} \widehat{\nabla u_h}\psi - \widehat{u_h}\nabla\psi\,\mathrm{d}S, \tag{3.9}$$

for all $\phi, \psi \in V_h^q, q \ge 1$. Then we have the following optimal initial error estimates for the time-dependent nonlinear Schrödinger equation (2.1)

$$\|\xi_u(\mathbf{x},0)\|_{L^2(\Omega_h)} + \|\xi_{ut}(\mathbf{x},0)\|_{L^2(\Omega_h)} + \|\xi_w(\mathbf{x},0)\|_{L^2(\Omega_h)} \le Ch^{q+1},$$

where C is a positive constant depending on q, the bounds of $F', F'', F^{(3)}$, $\|w(\mathbf{x},0)\|_{W^{2q+4}(\Omega_h)}$, $\|u(\mathbf{x},0)\|_{W^{2q+4}(\Omega_h)}$, $\|w(\mathbf{x},0)\|_{H^{q+1}(\Omega_h)}$, $\|u(\mathbf{x},0)\|_{H^{q+1}(\Omega_h)}$, $\|u_t(\mathbf{x},0)\|_{H^{q+1}(\Omega_h)}$ and $\|u(\mathbf{x},0)\|_{L^\infty(\Omega_h)}$ but not on h.

Proof. Let us first consider the DG approximation (3.8) and (3.9) for the numerical initial condition. We have the error identities

$$\int_K i e_u \phi \,\mathrm{d}\mathbf{x} + \mathcal{B}_K^1(e_w, \phi) = 0, \tag{3.10}$$

$$\int_K e_w \psi \,\mathrm{d}\mathbf{x} + \mathcal{B}_K^2(e_u, \psi) = 0, \tag{3.11}$$

where $e_u = u(\mathbf{x},0) - u_h(\mathbf{x},0)$, $e_w = w(\mathbf{x},0) - w_h(\mathbf{x},0)$, and $\mathcal{B}_K^1$ and $\mathcal{B}_K^2$ are defined in (2.7) and (2.8), respectively.

Multiply (3.10) by $-i$ and (3.11) by i with $(\phi,\psi) = (\xi_u^*, \xi_w^*)$. We take the complex conjugate of the resulting two equations and then sum them over all elements K to get

$$\begin{aligned} 2\sum_K \int_K |\xi_u|^2 + \mathrm{Re}(\eta_u \xi_u^*) - \mathrm{Im}(\eta_w \xi_w^*) \,\mathrm{d}\mathbf{x} \\ + i\sum_K -\mathcal{B}_K^1(\xi_w, \xi_u^*) + \mathcal{B}_K^2(\xi_u, \xi_w^*) + \mathcal{B}_K^1(\xi_w^*, \xi_u) - \mathcal{B}_K^2(\xi_u^*, \xi_w) \\ + i\sum_K -\mathcal{B}_K^1(\eta_w, \xi_u^*) + \mathcal{B}_K^2(\eta_u, \xi_w^*) + \mathcal{B}_K^1(\eta_w^*, \xi_u) - \mathcal{B}_K^2(\eta_u^*, \xi_w) = 0, \end{aligned} \tag{3.12}$$

where we have used the facts that $e_u = \xi_u + \eta_u$ and $e_w = \xi_w + \eta_w$. By the same arguments for the mass conservation (2.11) in Section 2.3, one has

$$\sum_K -\mathcal{B}_K^1(\xi_w, \xi_u^*) + \mathcal{B}_K^2(\xi_u, \xi_w^*) + \mathcal{B}_K^1(\xi_w^*, \xi_u) - \mathcal{B}_K^2(\xi_u^*, \xi_w) = 0.$$

Thanks to (3.4), one finds from (3.12) that

$$\begin{cases} 2\displaystyle\int_{\Omega_h} |\xi_u|^2 + \mathrm{Re}(\eta_u \xi_u^*) - \mathrm{Im}(\eta_w \xi_w^*) \,\mathrm{d}\mathbf{x} = 0, & d=1, \\ 2\displaystyle\int_{\Omega_h} |\xi_u|^2 + \mathrm{Re}(\eta_u \xi_u^*) - \mathrm{Im}(\eta_w \xi_w^*) \,\mathrm{d}\mathbf{x} \le Ch^{q+2}(\|\xi_u(\mathbf{x},0)\|_{L^2(\Omega_h)} + \|\xi_w(\mathbf{x},0)\|_{L^2(\Omega_h)}), & d=2, \end{cases}$$

where we have also used Lemma 1 to obtain the inequality when $d=2$. This yields

$$\|\xi_u(\mathbf{x},0)\|_{L^2(\Omega_h)}^2 \le Ch^{q+1}\big(\|\xi_u(\mathbf{x},0)\|_{L^2(\Omega_h)} + \|\xi_w(\mathbf{x},0)\|_{L^2(\Omega_h)}\big). \tag{3.13}$$

Similarly, choosing $\phi = \xi_u^*$ in (3.10), $\psi = \xi_w^*$ in (3.11), and taking the complex conjugate of the resulting two equations, then summing them over all elements K gives rise to

$$\begin{aligned} 2\sum_K \int_K |\xi_w|^2 - \mathrm{Im}(\eta_u \xi_u^*) + \mathrm{Re}(\eta_w \xi_w^*) \,\mathrm{d}\mathbf{x} \\ + \sum_K \mathcal{B}_K^1(\xi_w, \xi_u^*) + \mathcal{B}_K^2(\xi_u, \xi_w^*) + \mathcal{B}_K^1(\xi_w^*, \xi_u) + \mathcal{B}_K^2(\xi_u^*, \xi_w) \\ + \sum_K \mathcal{B}_K^1(\eta_w, \xi_u^*) + \mathcal{B}_K^2(\eta_u, \xi_w^*) + \mathcal{B}_K^1(\eta_w^*, \xi_u) + \mathcal{B}_K^2(\eta_u^*, \xi_w) = 0. \end{aligned}$$

Again, thanks to (3.4), we apply the same arguments for (2.12) to obtain that

$$\|\xi_w(\mathbf{x},0)\|_{L^2(\Omega_h)}^2 \le Ch^{q+1}\Big(\|\xi_u(\mathbf{x},0)\|_{L^2(\Omega_h)} + \|\xi_w(\mathbf{x},0)\|_{L^2(\Omega_h)}\Big). \tag{3.14}$$

Combining (3.13) and (3.14) and using Young's inequality, we arrive at

$$\|\xi_u(\mathbf{x},0)\|_{L^2(\Omega_h)} + \|\xi_w(\mathbf{x},0)\|_{L^2(\Omega_h)} \le Ch^{q+1}. \tag{3.15}$$

Next, we estimate $\|\xi_{ut}(\mathbf{x},0)\|_{L^2(\Omega_h)}$ by using the relation between the time dependent equation (2.9) and steady state equation (3.8). To this end, we start from the initial error equation for the time-dependent problem (2.9)

$$\int_K ie_{ut}\phi\,\mathrm{d}\mathbf{x} + \mathcal{B}_K^1(e_w,\phi) + \int_K uF'\big(|u|^2\big)\phi - u_hF'\big(|u_h|^2\big)\phi\,\mathrm{d}\mathbf{x} = 0,$$

where $\mathcal{B}_K^1$ is defined in (2.7). Subtracting this identity from (3.10) gives

$$\int_K ie_{ut}\phi - ie_u\phi + uF'\big(|u|^2\big)\phi - u_hF'\big(|u_h|^2\big)\phi\,\mathrm{d}\mathbf{x} = 0.$$

Multiplying the above equation by i, then choosing $\phi = \xi_{ut}^*$ and summing it over all elements K, we arrive at

$$\int_{\Omega_h} |\xi_{ut}|^2\,\mathrm{d}\mathbf{x} = \sum_K \int_K -\eta_{ut}\xi_{ut}^* + e_u\xi_{ut}^* + i\big(uF'\big(|u|^2\big)\xi_{ut}^* - u_hF'\big(|u_h|^2\big)\xi_{ut}^*\big)\,\mathrm{d}\mathbf{x}. \tag{3.16}$$

To estimate the right-hand side, we first apply (3.4) and (3.15) to have

$$\left|\sum_K \int_K -\eta_{ut}(\mathbf{x},0)\xi_{ut}^*(\mathbf{x},0) + e_u(\mathbf{x},0)\xi_{ut}^*(\mathbf{x},0)\,\mathrm{d}\mathbf{x}\right| \le Ch^{q+1}\|\xi_{ut}(\mathbf{x},0)\|_{L^2(\Omega_h)}. \tag{3.17}$$

To estimate the nonlinear terms on the right-hand side of (3.16), we have from the Taylor expansion that for some $|\hat{u}|^2$ between $|u|^2$ and $|u_h|^2$

$$F'\big(|u_h|^2\big) = F'\big(|u|^2\big) + F''\big(|u|^2\big)\gamma + \frac{1}{2}F'''\big(|\hat{u}|^2\big)\gamma^2, \tag{3.18}$$

where

$$\gamma := |u_h|^2 - |u|^2 = u_hu_h^* - uu^* = (u-e_u)(u^*-e_u^*) - uu^* = |e_u|^2 - 2\mathrm{Re}(u^*e_u). \tag{3.19}$$

Finally, we obtain

$$\begin{aligned}\left|\sum_K \int_K i\big(uF'\big(|u|^2\big) - u_hF'\big(|u_h|^2\big)\big)\xi_{ut}^*\,\mathrm{d}\mathbf{x}\right| &\le \left|\sum_K \int_K u\Big(-F''\big(|u|^2\big)\gamma - \frac{1}{2}F'''\big(|\hat{u}|^2\big)\gamma^2\Big)\xi_{ut}^*\,\mathrm{d}\mathbf{x}\right| \\ &\quad + \left|\sum_K \int_K e_u\Big(F'\big(|u|^2\big) + F''(|u|^2)\gamma + \frac{1}{2}F'''\big(|\hat{u}|^2\big)\gamma^2\Big)\xi_{ut}^*\,\mathrm{d}\mathbf{x}\right| \\ &\le Ch^{q+1}\|\xi_{ut}(\mathbf{x},0)\|_{L^2(\Omega_h)}.\end{aligned} \tag{3.20}$$

After combining (3.16), (3.17) with (3.20), we find that $\|\xi_{ut}(\mathbf{x},0)\|_{L^2(\Omega_h)} \le Ch^{q+1}$ and this completes the proof. ☐

3.4. Optimal error estimates

We are now ready to present error estimates for the DG scheme (2.9) and (2.10) with the numerical fluxes (3.1). In particular, we will show that the estimates are optimal in the L^2 norm.

Theorem 2. *Assume that $F \in C^{4,\zeta}(\mathbb{R})$ for some $\zeta \in (0,1)$, and let (u,w) be the sufficiently smooth solution to system (2.2) and $(u_h,w_h) \in V_h^q \times V_h^q, q \ge 1$ be the numerical solution of the DG scheme (2.9) and (2.10) with the smooth initial data computed by (3.8) and (3.9) along with periodic boundary conditions and the numerical fluxes (3.1), then we have the following error estimates:*

$$\|e_u(\mathbf{x},t)\|_{L^2(\Omega_h)} + \|e_w(\mathbf{x},t)\|_{L^2(\Omega_h)} + \|e_{ut}(\mathbf{x},t)\|_{L^2(\Omega_h)} \le Ch^{q+1} \qquad \forall 0 \le t \le T, \tag{3.21}$$

where the positive constant C depends on q, the bounds of $F', F'', F^{(3)}, F^{(4)}$, $\|u_{tt}\|_{L^\infty([0,T],H^{q+1}(\Omega_h))}$, $\|u_t\|_{L^\infty([0,T],H^{q+1}(\Omega_h))}$, $\|w_t\|_{L^\infty([0,T],H^{q+1}(\Omega_h))}$, $\|w\|_{L^\infty([0,T],H^{q+1}(\Omega_h))}$, $\|u\|_{L^\infty([0,T],H^{q+1}(\Omega_h))}$, $\|u\|_{L^\infty([0,T],W^{2q+4}(\Omega_h))}$, $\|w\|_{L^\infty([0,T],W^{2q+4}(\Omega_h))}$, $\|u_t\|_{L^\infty([0,T],W^{2q+4}(\Omega_h))}$, but not h.

Proof. Our proof consists of three steps: (i) the estimate of $\mathrm{d}\|\xi_u\|_{L^2(K)}/\mathrm{d}t$, (ii) the estimate of $\mathrm{d}\|\xi_w\|_{L^2(K)}/\mathrm{d}t$, and (iii) the estimate of $\mathrm{d}\|\xi_{ut}\|_{L^2(K)}/\mathrm{d}t$.

Step one: by the DG scheme (2.9) and (2.10), we have the following error equations for any $(\phi,\psi)\in V_h^q\times V_h^q$

$$\int_K e_{ut}\phi\,\mathrm{d}\mathbf{x} - i\int_K uF'\big(|u|^2\big)\phi - u_hF'\big(|u_h|^2\big)\phi\,\mathrm{d}\mathbf{x} - i\mathcal{B}_K^1(e_w,\phi)=0 \tag{3.22}$$

and

$$\int_K ie_w\psi\,\mathrm{d}\mathbf{x} + i\mathcal{B}_K^2(e_u,\psi)=0, \tag{3.23}$$

where $\mathcal{B}_K^1$ and $\mathcal{B}_K^2$ are defined in (2.7) and (2.8), respectively. Choosing $\phi=\xi_u^*$ and $\psi=\xi_w^*$ in (3.22) and (3.23), and taking the complex conjugate, then adding them with the resulting two equations and summing over all elements K yields

$$\begin{aligned}\frac{\mathrm{d}}{\mathrm{d}t}\sum_K\int_K|\xi_u|^2\,\mathrm{d}\mathbf{x} &= \overbrace{\sum_K\int_K -2\mathrm{Re}(\eta_{ut}\xi_u^*)\ +2\mathrm{Im}(\eta_w\xi_w^*)\,\mathrm{d}\mathbf{x}}^{:=\Lambda_1}\\ &\quad+\overbrace{i\sum_K -\mathcal{B}_K^2(\xi_u,\xi_w^*)+\mathcal{B}_K^2(\xi_u^*,\xi_w)+\mathcal{B}_K^1(\xi_w,\xi_u^*)-\mathcal{B}_K^1(\xi_w^*,\xi_u)}^{:=\Lambda_2}\\ &\quad+\overbrace{i\sum_K -\mathcal{B}_K^2(\eta_u,\xi_w^*)+\mathcal{B}_K^2(\eta_u^*,\xi_w)+\mathcal{B}_K^1(\eta_w,\xi_u^*)-\mathcal{B}_K^1(\eta_w^*,\xi_u)}^{:=\Lambda_3}\\ &\quad+\overbrace{\sum_K\int_K -2F'\big(|u|^2\big)\mathrm{Im}\big(u\xi_u^*\big)+2F'\big(|u_h|^2\big)\mathrm{Im}\big(u_h\xi_u^*\big)\,\mathrm{d}\mathbf{x}}^{:=\Lambda_4},\end{aligned} \tag{3.24}$$

where we have used the identities $e_u=\eta_u+\xi_u$ and $e_w=\eta_w+\xi_w$.

First of all, we infer from (3.4) that

$$|\Lambda_1|\le Ch^{q+1}\big(\|\xi_u\|_{L^2(\Omega_h)}+\|\xi_w\|_{L^2(\Omega_h)}\big), \tag{3.25}$$

and the same arguments for the mass conservation (2.11) lead us to

$$\Lambda_2=0. \tag{3.26}$$

To estimate Λ_3, we infer from the definition of the projection operators $\mathbb{P}_h^{\pm}$, the numerical fluxes (3.1) and Lemma 1, we obtain

$$\begin{cases}|\Lambda_3|=0, & d=1,\\ |\Lambda_3|\le Ch^{q+2}\big(\|\xi_u\|_{L^2(\Omega_h)}+\|\xi_w\|_{L^2(\Omega_h)}\big), & d=2.\end{cases} \tag{3.27}$$

Finally, to estimate Λ_4, we first apply (3.18) and (3.19) to rewrite it as

$$\begin{aligned}\Lambda_4 &= -2\sum_K\int_K\big(F'\big(|u|^2\big)-F'\big(|u_h|^2\big)\big)\mathrm{Im}\big(u\xi_u^*\big)+F'\big(|u_h|^2\big)\mathrm{Im}\big(e_u\xi_u^*\big)\,\mathrm{d}\mathbf{x}\\ &=2\Bigg(\overbrace{\sum_K\int_K\Big(F''\big(|u|^2\big)\gamma+\frac{1}{2}F'''\big(|\hat{u}|^2\big)\gamma^2\Big)\mathrm{Im}\big(u\xi_u^*\big)\,\mathrm{d}\mathbf{x}}^{:=\Lambda_{41}}\end{aligned}$$

$$\left.\overbrace{-\sum_K \int_K \Big(F'\big(|u|^2\big) + F''\big(|u|^2\big)\gamma + \frac{1}{2}F'''\big(|\hat{u}|^2\big)\gamma^2\Big)\mathrm{Im}\big(e_u\xi_u^*\big)\,\mathrm{d}\mathbf{x}}^{:=\Lambda_{42}}\right).$$

On the one hand, we apply

$$\int_K |\gamma \mathrm{Im}(u\xi_u^*)|\,\mathrm{d}\mathbf{x} \le C\Big(\|u\|_{L^\infty(K)}\|e_u\|_{L^\infty(K)} + \|u\|^2_{L^\infty(K)}\Big)\Big(\|\xi_u\|^2_{L^2(K)} + \|\eta_u\|^2_{L^2(K)}\Big),$$

to see that

$$\begin{aligned}|\Lambda_{41}| \le\ & C\big(\|F''\|_{L^\infty(\Omega_h)} + \|\gamma\|_{L^\infty(\Omega_h)}\|F'''\|_{L^\infty(\Omega_h)}\big)\\ &\cdot \Big(\|u\|_{L^\infty(\Omega_h)}\|e_u\|_{L^\infty(\Omega_h)} + \|u\|^2_{L^\infty(\Omega_h)}\Big)\Big(\|\xi_u\|^2_{L^2(\Omega_h)} + \|\eta_u\|^2_{L^2(\Omega_h)}\Big).\end{aligned}$$

On the other hand, we have $\mathrm{Im}(e_u\xi_u^*) = \mathrm{Im}(\eta_u\xi_u^*)$ since $\xi_u\xi_u^* = |\xi_u|^2$ is a real number, then

$$|\Lambda_{42}| \le C\big(\|F'\|_{L^\infty(\Omega_h)} + \|\gamma\|_{L^\infty(\Omega_h)}\|F''\|_{L^\infty(\Omega_h)} + \|\gamma^2\|_{L^\infty(\Omega_h)}\|F'''\|_{L^\infty(\Omega_h)}\big)\Big(\|\xi_u\|^2_{L^2(\Omega_h)} + \|\eta_u\|^2_{L^2(\Omega_h)}\Big).$$

Combining the bounds of Λ_{41} and Λ_{42} derived above, we get

$$\begin{aligned}|\Lambda_4| \le\ & C\Big(\big(\|F''\|_{L^\infty(\Omega_h)} + \|\gamma\|_{L^\infty(\Omega_h)}\|F'''\|_{L^\infty(\Omega_h)}\big)\cdot\Big(\|u\|_{L^\infty(\Omega_h)}\|e_u\|_{L^\infty(\Omega_h)} + \|u\|^2_{L^\infty(\Omega_h)}\Big)\\ &+ \|F'\|_{L^\infty(\Omega_h)} + \|\gamma\|_{L^\infty(\Omega_h)}\|F''\|_{L^\infty(\Omega_h)} + \|\gamma^2\|_{L^\infty(\Omega_h)}\|F'''\|_{L^\infty(\Omega_h)}\Big)\\ &\cdot\Big(\|\xi_u\|^2_{L^2(\Omega_h)} + \|\eta_u\|^2_{L^2(\Omega_h)}\Big),\end{aligned} \tag{3.28}$$

and this, in the light of (3.6), further implies that

$$\|\gamma\|_{L^\infty(\Omega_h)} \le C\big(1 + \|u\|_{L^\infty(\Omega_h)}\big),\quad \|\gamma^2\|_{L^\infty(\Omega_h)} \le C\Big(1 + \|u\|_{L^\infty(\Omega_h)} + \|u\|^2_{L^\infty(\Omega_h)}\Big). \tag{3.29}$$

Then we have from (3.28) and (3.29) that

$$|\Lambda_4| \le C\Big(\|\xi_u\|^2_{L^2(\Omega_h)} + \|\eta_u\|^2_{L^2(\Omega_h)}\Big). \tag{3.30}$$

Finally, after plugging (3.25)–(3.27) and (3.30) into (3.24) and using Young's inequality, we have

$$\frac{\mathrm{d}}{\mathrm{d}t}\|\xi_u\|^2_{L^2(\Omega_h)} \le C\Big(\|\xi_u\|^2_{L^2(\Omega_h)} + \|\xi_w\|^2_{L^2(\Omega_h)} + h^{2(q+1)}\Big). \tag{3.31}$$

Step two: we differentiate (2.10) with respect to time and then apply (2.9) to obtain that, for any $(\phi,\psi) \in V_h^q \times V_h^q$

$$i\int_K e_{ut}\phi\,\mathrm{d}\mathbf{x} + \int_K uF'\big(|u|^2\big)\phi - u_hF'\big(|u_h|^2\big)\phi\,\mathrm{d}\mathbf{x} + \mathcal{B}_K^1(e_w,\phi) = 0 \tag{3.32}$$

and

$$\int_K e_{wt}\psi\,\mathrm{d}\mathbf{x} + \mathcal{B}_K^2(e_{ut},\psi) = 0. \tag{3.33}$$

Here, $\mathcal{B}_K^1$ and $\mathcal{B}_K^2$ are defined in (2.7) and (2.8), respectively. Choose $\phi = \xi_{ut}^*$, $\psi = \xi_w^*$ in (3.32) and (3.33) and take the complex conjugate. We then add them to the resulting two equations and sum it over all elements K to find that

$$
\begin{aligned}
\frac{\mathrm{d}}{\mathrm{d}t}\sum_K\int_K|\xi_w|^2\,\mathrm{d}\mathbf{x} = &\overbrace{\sum_K\int_K 2\mathrm{Im}(\eta_{ut}\xi_{ut}^*) - 2\mathrm{Re}(\eta_{wt}\xi_w^*)\,\mathrm{d}\mathbf{x}}^{:=\Theta_1}\\
&\overbrace{-\sum_K \mathcal{B}_K^1(\xi_w,\xi_{ut}^*) + \mathcal{B}_K^1(\xi_w^*,\xi_{ut}) + \mathcal{B}_K^2(\xi_{ut},\xi_w^*) + \mathcal{B}_K^2(\xi_{ut}^*,\xi_w)}^{:=\Theta_2}\\
&\overbrace{-\sum_K \mathcal{B}_K^1(\eta_w,\xi_{ut}^*) + \mathcal{B}_K^1(\eta_w^*,\xi_{ut}) + \mathcal{B}_K^2(\eta_{ut},\xi_w^*) + \mathcal{B}_K^2(\eta_{ut}^*,\xi_w)}^{:=\Theta_3}\\
&\overbrace{-\sum_K\int_K 2F'\big(|u|^2\big)\mathrm{Re}\big(u\xi_{ut}^*\big) - 2F'\big(|u_h|^2\big)\mathrm{Re}\big(u_h\xi_{ut}^*\big)\,\mathrm{d}\mathbf{x}}^{:=\Theta_4},
\end{aligned}
\tag{3.34}
$$

where we use the identities $e_u = \eta_u + \xi_u$ and $e_w = \eta_w + \xi_w$.

Similar to step one, we get

$$
|\Theta_1| \le Ch^{q+1}\Big(\|\xi_{ut}\|_{L^2(\Omega_h)} + \|\xi_w\|_{L^2(\Omega_h)}\Big), \quad |\Theta_4| \le C\Big(\|\xi_{ut}\|^2_{L^2(\Omega_h)} + \|\xi_u\|^2_{L^2(\Omega_h)} + \|\eta_u\|^2_{L^2(\Omega_h)}\Big),
$$

and

$$
\begin{cases}
|\Theta_3| = 0, & d=1,\\
|\Theta_3| \le Ch^{q+2}\big(\|\xi_{ut}\|_{L^2(\Omega_h)} + \|\xi_w\|_{L^2(\Omega_h)}\big), & d=2.
\end{cases}
$$

Moreover, the same arguments for the Hamiltonian conservation (2.12) in Theorem 1 give us

$$
\Theta_2 = 0.
$$

Substituting the estimates of $|\Theta_3|$ into (3.34) and then using Young's inequality, we have

$$
\frac{\mathrm{d}}{\mathrm{d}t}\|\xi_w\|^2_{L^2(\Omega_h)} \le C\Big(\|\xi_u\|^2_{L^2(\Omega_h)} + \|\xi_{ut}\|^2_{L^2(\Omega_h)} + \|\xi_w\|^2_{L^2(\Omega_h)} + h^{2(q+1)}\Big).
\tag{3.35}
$$

Note that $\|\xi_{ut}\|^2_{L^2(\Omega_h)}$ in (3.35) is unknown, and we need to estimate it to estimate $\mathrm{d}\|\xi_w\|^2_{L^2(\Omega_h)}/\mathrm{d}t$.

Step three: taking the time derivative of (2.9) and (2.10) we get the following error equations

$$
\int_K e_{utt}\phi\,\mathrm{d}\mathbf{x} - i\int_K \frac{\mathrm{d}}{\mathrm{d}t}\big(uF'\big(|u|^2\big)\phi - u_hF'\big(|u_h|^2\big)\big)\phi\,\mathrm{d}\mathbf{x} - i\mathcal{B}_K^1\big(e_{wt},\phi\big) = 0,
\tag{3.36}
$$

$$
\int_K ie_{wt}\psi\,\mathrm{d}\mathbf{x} + i\mathcal{B}_K^2(e_{ut},\psi) = 0,
\tag{3.37}
$$

for any $(\phi,\psi)\in V_h^q\times V_h^q$, and $\mathcal{B}_K^1$, $\mathcal{B}_K^2$ are defined in (2.7) and (2.8), respectively. Choosing $\phi = \xi_{ut}^*$, $\psi = \xi_{wt}^*$ in (3.36) and (3.37), and taking their complex conjugate, then adding them with the resulting two equations and summing over all elements K, we have

$$
\begin{aligned}
\frac{\mathrm{d}}{\mathrm{d}t}\sum_K\int_K|\xi_{ut}|^2\,\mathrm{d}\mathbf{x} = &\overbrace{\sum_K\int_K -2\mathrm{Re}(\eta_{utt}\xi_{ut}^*)\,\mathrm{d}\mathbf{x}}^{:=W_1}\\
&+i\overbrace{\sum_K \mathcal{B}_K^2(\xi_{ut}^*,\xi_{wt}) - \mathcal{B}_K^2(\xi_{ut},\xi_{wt}^*) + \mathcal{B}_K^1(\xi_{wt},\xi_{ut}^*) - \mathcal{B}_K^1(\xi_{wt}^*,\xi_{ut})}^{:=W_2}
\end{aligned}
$$

$$
+\, i \overbrace{\sum_K \mathcal{B}_K^1(\eta_{wt}, \xi_{ut}^*) - \mathcal{B}_K^1(\eta_{wt}^*, \xi_{ut})}^{:=W_3}
$$

$$
+\, i \overbrace{\sum_K \int_K \frac{\mathrm{d}}{\mathrm{d}t}\big(uF'(|u|^2) - u_h F'(|u_h|^2)\big)\xi_{ut}^* - \frac{\mathrm{d}}{\mathrm{d}t}\Big(u^* F'(|u|^2) - u_h^* F'(|u_h|^2)\Big)\xi_{ut}\,\mathrm{d}\mathbf{x}}^{:=W_4}
$$

$$
+\, i \overbrace{\sum_K \mathcal{B}_K^2(\eta_{ut}^*, \xi_{wt}) - \mathcal{B}_K^2(\eta_{ut}, \xi_{wt}^*)}^{:=W_5} + \overbrace{\sum_K \int_K 2\mathrm{Im}(\eta_{wt}\xi_{wt}^*)\,\mathrm{d}\mathbf{x}}^{:=W_6}. \tag{3.38}
$$

By similar analysis as in step one, we have

$$
|W_1| \le Ch^{q+1}\|\xi_{ut}\|_{L^2(\Omega_h)}, \quad W_2 = 0, \tag{3.39}
$$

and

$$
\begin{cases} |W_3 + W_5| = 0, & d = 1, \\ |W_3| \le Ch^{q+2}\|\xi_{ut}\|_{L^2(\Omega_h)}, & d = 2. \end{cases} \tag{3.40}
$$

To estimate W_4, we first rewrite it into

$$
W_4 = -2\Bigg(\overbrace{\sum_K \int_K \big(F'(|u|^2) - F'(|u_h|^2)\big)\mathrm{Im}(u_t\xi_{ut}^*) + F'(|u_h|^2)\mathrm{Im}(e_{ut}\xi_{ut}^*)\,\mathrm{d}\mathbf{x}}^{:=W_{41}}
$$

$$
+ \overbrace{\sum_K \int_K \left(F''(|u|^2)\frac{\mathrm{d}|u|^2}{\mathrm{d}t} - F''(|u_h|^2)\frac{\mathrm{d}|u_h|^2}{\mathrm{d}t}\right)\mathrm{Im}\big(u\xi_{ut}^*\big) + F''(|u_h|^2)\frac{\mathrm{d}|u_h|^2}{\mathrm{d}t}\mathrm{Im}(e_u\xi_{ut}^*)\,\mathrm{d}\mathbf{x}}^{:=W_{42}}\Bigg). \tag{3.41}
$$

Then the same estimates for Λ_4 in step one imply that

$$
|W_{41}| \le C\Big(\|\xi_u\|_{L^2(\Omega_h)}^2 + \|\xi_{ut}\|_{L^2(\Omega_h)}^2 + \|\eta_u\|_{L^2(\Omega_h)}^2 + \|\eta_{ut}\|_{L^2(\Omega_h)}^2\Big). \tag{3.42}
$$

To estimate W_{42}, we find for some $|\underline{u}|^2$ between $|u|^2$ and $|u_h|^2$ that

$$
F''(|u_h|^2) = F''(|u|^2) + F'''(|u|^2)\gamma + \frac{1}{2}F^{(4)}(|\underline{u}|^2)\gamma^2,
$$

where γ is defined in (3.19); moreover, we divide W_{42} into two parts as follows

$$
W_{42} = \overbrace{\sum_K \int_K \left(-F''(|u|^2)\frac{\mathrm{d}\gamma}{\mathrm{d}t} - \left(F'''(|u|^2)\gamma + \frac{1}{2}F^{(4)}(|\underline{u}|^2)\gamma^2\right)\left(\frac{\mathrm{d}|u|^2}{\mathrm{d}t} + \frac{\mathrm{d}\gamma}{\mathrm{d}t}\right)\right)\mathrm{Im}(u\xi_{ut}^*)\,\mathrm{d}\mathbf{x}}^{:=W_{42}^{(1)}}
$$

$$
+ \overbrace{\sum_K \int_K \left(F''(|u|^2) + F'''(|u|^2)\gamma + \frac{1}{2}F^{(4)}(|\underline{u}|^2)\gamma^2\right)\left(\frac{\mathrm{d}|u|^2}{\mathrm{d}t} + \frac{\mathrm{d}\gamma}{\mathrm{d}t}\right)\mathrm{Im}(e_u\xi_{ut}^*)\,\mathrm{d}\mathbf{x}}^{:=W_{42}^{(2)}}. \tag{3.43}
$$

Thanks to (3.6), we obtain that

$$\begin{aligned}\left|W_{42}^{(1)}\right| \le C\Bigg(&\|F''\|_{L^\infty(\Omega_h)}\left(1+\|u\|_{L^\infty(\Omega_h)}+\left\|\frac{\mathrm{d}u}{\mathrm{d}t}\right\|_{L^\infty(\Omega_h)}\right)+\big[\|F'''\|_{L^\infty(\Omega_h)}\big(1+\|u\|_{L^\infty(\Omega_h)}\big)\\
&+\left\|F^{(4)}\right\|_{L^\infty(\Omega_h)}\|\gamma\|_{L^\infty(\Omega_h)}\big(1+\|u\|_{L^\infty(\Omega_h)}\big)\big]\left(\left\|\frac{\mathrm{d}|u|^2}{\mathrm{d}t}\right\|_{L^\infty(\Omega_h)}+\left\|\frac{\mathrm{d}\gamma}{\mathrm{d}t}\right\|_{L^\infty(\Omega_h)}\right)\Bigg)\\
&\cdot\|u\|_{L^\infty(\Omega_h)}\Big(\|\xi_{ut}\|^2_{L^2(\Omega_h)}+\|\xi_u\|^2_{L^2(\Omega_h)}+\|\eta_u\|^2_{L^2(\Omega_h)}+\|\eta_{ut}\|^2_{L^2(\Omega_h)}\Big),\end{aligned}\tag{3.44}$$

and

$$\begin{aligned}|W_{42}^{(2)}| \le C\Big(&\|F''\|_{L^\infty(\Omega_h)}+\|F'''\|_{L^\infty(\Omega_h)}\|\gamma\|_{L^\infty(\Omega_h)}+\|F^{(4)}\|_{L^\infty(\Omega_h)}\|\gamma^2\|_{L^\infty(\Omega_h)}\Big)\\
&\cdot\left(\left\|\frac{\mathrm{d}|u|^2}{\mathrm{d}t}\right\|_{L^\infty(\Omega_h)}+\left\|\frac{\mathrm{d}\gamma}{\mathrm{d}t}\right\|_{L^\infty(\Omega_h)}\right)\Big(\|\xi_u\|^2_{L^2(\Omega_h)}+\|\xi_{ut}\|^2_{L^2(\Omega_h)}+\|\eta_u\|^2_{L^2(\Omega_h)}\Big).\end{aligned}\tag{3.45}$$

In addition, using (3.19) and (3.6), we have

$$\left\|\frac{\mathrm{d}\gamma}{\mathrm{d}t}\right\|_{L^\infty(\Omega_h)} \le C\left(1+\|u\|_{L^\infty(\Omega_h)}+\left\|\frac{\mathrm{d}u}{\mathrm{d}t}\right\|_{L^\infty(\Omega_h)}\right).\tag{3.46}$$

Plugging (3.29) and (3.46) into (3.44) and (3.45), we have from (3.41) to (3.43) that

$$|W_4| \le C\Big(\|\xi_u\|^2_{L^2(\Omega_h)}+\|\xi_{ut}\|^2_{L^2(\Omega_h)}+h^{2(q+1)}\Big).\tag{3.47}$$

Substituting (3.39), (3.40) and (3.47) into (3.38) and using Young's inequality, we obtain

$$\frac{\mathrm{d}}{\mathrm{d}t}\|\xi_{ut}\|^2_{L^2(\Omega_h)} \le C\Big(\|\xi_u\|^2_{L^2(\Omega_h)}+\|\xi_{ut}\|^2_{L^2(\Omega_h)}+h^{2(q+1)}\Big)+|W_5|+|W_6|.\tag{3.48}$$

In 1D, $|W_3+W_5|=0$ according to (3.40). Then collecting (3.31), (3.35) and (3.48) leads us to

$$\begin{aligned}&\frac{\mathrm{d}}{\mathrm{d}t}\Big(\|\xi_u\|^2_{L^2(\Omega_h)}+\|\xi_w\|^2_{L^2(\Omega_h)}+\|\xi_{ut}\|^2_{L^2(\Omega_h)}\Big)\\
&\quad\le C\Big(\|\xi_u\|^2_{L^2(\Omega_h)}+\|\xi_w\|^2_{L^2(\Omega_h)}+\|\xi_{ut}\|^2_{L^2(\Omega_h)}\Big)+Ch^{2(q+1)}+|W_5|+|W_6|.\end{aligned}$$

We then integrate this inequality from 0 to T to find that

$$\begin{aligned}&\|\xi_u(\mathbf{x},T)\|^2_{L^2(\Omega_h)}+\|\xi_w(\mathbf{x},T)\|^2_{L^2(\Omega_h)}+\|\xi_{ut}(\mathbf{x},T)\|^2_{L^2(\Omega_h)}\\
&\quad\le \|\xi_u(\mathbf{x},0)\|^2_{L^2(\Omega_h)}+\|\xi_w(\mathbf{x},0)\|^2_{L^2(\Omega_h)}+\|\xi_{ut}(\mathbf{x},0)\|^2_{L^2(\Omega_h)}\\
&\qquad+C\int_0^T\|\xi_u\|^2_{L^2(\Omega_h)}+\|\xi_w\|^2_{L^2(\Omega_h)}+\|\xi_{ut}\|^2_{L^2(\Omega_h)}\,\mathrm{d}t+Ch^{2(q+1)}+\int_0^T|W_5|+|W_6|\,\mathrm{d}t.\end{aligned}\tag{3.49}$$

In 2D, we have from integration by parts that

$$\begin{aligned}\int_0^T|W_5|\,\mathrm{d}t&=\int_0^T\left|i\sum_K\mathcal{B}_K^2(\eta_{ut}^*,\xi_{wt})-\mathcal{B}_K^2(\eta_{ut},\xi_{wt}^*)\right|\mathrm{d}t\\
&\le\sum_K\left(\left|\mathcal{B}_K^2(\eta_{ut}^*,\xi_w)\right|+\left|\mathcal{B}_K^2(\eta_{ut},\xi_w^*)\right|\right)\Big|_0^T+\int_0^T\sum_K\left|\mathcal{B}_K^2(\eta_{utt}^*,\xi_w)\right|+\left|\mathcal{B}_K^2(\eta_{utt},\xi_w^*)\right|\mathrm{d}t.\end{aligned}\tag{3.50}$$

For $\int_0^T |W_6|\,\mathrm{d}t$, we integrate by part again to have that

$$\begin{aligned}\int_0^T |W_6|\,\mathrm{d}t &= \int_0^T \Big|\sum_K \int_K 2\mathrm{Im}(\eta_{wt}\xi_{wt}^*)\mathrm{d}\mathbf{x}\Big|\,\mathrm{d}t\\ &\le \sum_K \int_K \Big|2\mathrm{Im}(\eta_{wt}\xi_w^*)\Big|\,\mathrm{d}\mathbf{x}\Big|_0^T + \int_0^T \sum_K \int_K \Big|2\mathrm{Im}(\eta_{wtt}\xi_w^*)\Big|\,\mathrm{d}t. \end{aligned} \tag{3.51}$$

After substituting (3.50) and (3.51) into (3.49), we invoke Young's inequality and Lemma 1 to find

$$\begin{aligned}&\|\xi_u(\mathbf{x},T)\|^2_{L^2(\Omega_h)} + \|\xi_w(\mathbf{x},T)\|^2_{L^2(\Omega_h)} + \|\xi_{ut}(\mathbf{x},T)\|^2_{L^2(\Omega_h)}\\ &\qquad\le C\int_0^T \|\xi_u\|^2_{L^2(\Omega_h)} + \|\xi_w\|^2_{L^2(\Omega_h)} + \|\xi_{ut}\|^2_{L^2(\Omega_h)}\,\mathrm{d}t + Ch^{2(q+1)} + \frac{1}{2}\|\xi_w(\mathbf{x},T)\|^2_{L^2(\Omega_h)}. \end{aligned} \tag{3.52}$$

Finally, using the Grönwall's inequality (3.52) gives rise to

$$\|\xi_u(\mathbf{x},T)\|^2_{L^2(\Omega_h)} + \|\xi_w(\mathbf{x},T)\|^2_{L^2(\Omega_h)} + \|\xi_{ut}(\mathbf{x},T)\|^2_{L^2(\Omega_h)} \le Ch^{2(q+1)},$$

which then easily implies the error estimate (3.21) using (3.4) and the triangle inequality. □

Remark 3. When $F'(|u|^2) \equiv$ constant, one has the same estimates without assuming (3.5).

3.5. Verification of the *a priori* error estimate

We are now left to verify the *a priori* error estimate assumption (3.5). To see this, we first find that (3.5) is true at $t = 0$ thanks to Lemma 2. To show it for all $t > 0$, we argue by contradiction. First, for each $q \ge 1$, we have $Ch^{q+1} < h$ if h is small enough. Suppose (3.5) fails before T, namely, there exists some $t_* \in (0,T)$ such that $t_* = \inf\{t : \|(u-u_h)(\cdot,t)\|_{L^2(\Omega_h)} + \|(u_t-u_{ht})(\cdot,t)\|_{L^2(\Omega_h)} > h\}$. By the continuity of $\|(u-u_h)(\cdot,t)\|_{L^2(\Omega_h)} + \|(u_t-u_{ht})(\cdot,t)\|_{L^2(\Omega_h)}$, we have $h = \|(u-u_h)(\cdot,t_*)\|_{L^2(\Omega_h)} + \|(u_t-u_{ht})(\cdot,t_*)\|_{L^2(\Omega_h)}$. On the other hand, equation (3.5) holds for $0 \le t \le t_*$, thus from Theorem 2, we have $\|(u-u_h)(\cdot,t_*)\|_{L^2(\Omega_h)} + \|(u_t-u_{ht})(\cdot,t_*)\|_{L^2(\Omega_h)} \le Ch^{q+1}$, which is a contradiction when $q \ge 1$. Therefore, we have $\|(u-u_h)(\cdot,t)\|_{L^2(\Omega_h)} + \|(u_t-u_{ht})(\cdot,t)\|_{L^2(\Omega_h)} \le h$ for all $t \in (0,T)$, and this verifies (3.5).

4. Time discretization

In this section, we extend the semi-discrete ultraweak-local DG method to the fully discrete method, which preserves the fully discrete mass and the fully discrete Hamiltonian.

4.1. Crank–Nicolson time discretization

We study the Crank–Nicolson scheme for time and show the mass and Hamiltonian conservation properties of the corresponding fully discrete scheme. Let $0 = t_0 < t_1 < \cdots < t_n < \cdots < \cdots < t_{N_t} = T$ and denote $h_t := t_{n+1} - t_n$. Here we use the uniform time step h_t and denote the DG solution at $t = t_n$ by u_h^n. We also introduce the following two operators, which will be used in the rest of the content

$$\texttt{central difference operator}: \delta u^n = \frac{u^{n+1} - u^{n-1}}{2h_t},$$

and

$$\texttt{mean value operator}: \bar{\delta} u^n = \frac{u^{n+1} + u^{n-1}}{2}.$$

The fully discrete approximation $u_h^n = u(\cdot, t_n)$ of problem (2.2) satisfies

$$\int_K i\delta u_h^n \phi + \bar{\delta} w_h^n \Delta\phi + \bar{\delta} u_h^n \mathcal{G}\phi \,\mathrm{d}\mathbf{x} = \int_{\partial K} -\bar{\delta}\widetilde{\nabla w_h^n}\cdot \mathbf{n}\phi + \bar{\delta}\widetilde{w_h^n}\nabla\phi\cdot\mathbf{n}\,\mathrm{d}S, \tag{4.1}$$

$$\int_K w_h^{n+1}\psi - u_h^{n+1}\Delta\psi \,\mathrm{d}\mathbf{x} = \int_{\partial K} \widehat{\nabla u_h^{n+1}}\cdot\mathbf{n}\psi - \widehat{u_h^{n+1}}\nabla\psi\cdot\mathbf{n}\,\mathrm{d}S, \tag{4.2}$$

$$\int_K w_h^{n-1}\psi - u_h^{n-1}\Delta\psi \,\mathrm{d}\mathbf{x} = \int_{\partial K} \widehat{\nabla u_h^{n-1}}\cdot\mathbf{n}\psi - \widehat{u_h^{n-1}}\nabla\psi\cdot\mathbf{n}\,\mathrm{d}S, \tag{4.3}$$

for all test functions $\phi, \psi \in V_h^q$, where $\mathcal{G} = \frac{F\left(|u_h^{n+1}|^2\right) - F\left(|u_h^{n-1}|^2\right)}{|u_h^{n+1}|^2 - |u_h^{n-1}|^2}$ and the numerical fluxes are defined in (3.1). We then have the following conservation property.

Theorem 3. *For all n, the solution to the fully discrete ultraweak-local DG scheme (4.1)–(4.3) conserves the discrete mass*

$$M_h^{n+1} := \frac{1}{2}\sum_K \int_K |u_h^n| + \left|u_h^{n+1}\right| \mathrm{d}\mathbf{x}, \tag{4.4}$$

and the discrete Hamiltonian

$$H_h^{n+1} := \frac{1}{2}\sum_K \int_K |w_h^n| + \left|w_h^{n+1}\right| + F\left(|u_h^{n+1}|^2\right) + F\left(|u_h^n|^2\right)\mathrm{d}\mathbf{x}. \tag{4.5}$$

Proof. To prove the fully discrete mass conservation (4.4), we choose the test function $\phi = \bar{\delta} u_h^{n,*}$ in (4.1) to obtain

$$\int_K i\delta u_h^n \bar{\delta} u_h^{n,*} + \bar{\delta} w_h^n \Delta\bar{\delta} u^{n,*} + \bar{\delta} u_h^n \mathcal{G}\bar{\delta} u_h^{n,*} \,\mathrm{d}\mathbf{x} = \int_{\partial K} -\bar{\delta}\widetilde{\nabla w_h^n}\cdot\mathbf{n}\bar{\delta} u_h^{n,*} + \bar{\delta}\widetilde{w_h^n}\nabla\bar{\delta} u_h^{n,*}\cdot\mathbf{n}\,\mathrm{d}S, \tag{4.6}$$

and the test function $\psi = \bar{\delta} w_h^{n,*}/2$ in (4.2) and (4.3) to obtain

$$\int_K \left(w_h^{n+1}\bar{\delta} w_h^{n,*} - u_h^{n+1}\Delta\bar{\delta} w_h^{n,*}\right)/2\,\mathrm{d}\mathbf{x} = \int_{\partial K}\left(\widehat{\nabla u_h^{n+1}}\cdot\mathbf{n}\bar{\delta} w_h^{n,*} - \widehat{u_h^{n+1}}\nabla\bar{\delta} w_h^{n,*}\cdot\mathbf{n}\right)/2\,\mathrm{d}S, \tag{4.7}$$

and

$$\int_K \left(w_h^{n-1}\bar{\delta} w_h^{n,*} - u_h^{n-1}\Delta\bar{\delta} w_h^{n,*}\right)/2\,\mathrm{d}\mathbf{x} = \int_{\partial K}\left(\widehat{\nabla u_h^{n-1}}\cdot\mathbf{n}\bar{\delta} w_h^{n,*} - \widehat{u_h^{n-1}}\nabla\bar{\delta} w_h^{n,*}\cdot\mathbf{n}\right)/2\,\mathrm{d}S. \tag{4.8}$$

Adding (4.7) and (4.8), we have

$$\int_K \bar{\delta} w_h^n \bar{\delta} w_h^{n,*} - \bar{\delta} u_h^n \Delta\bar{\delta} w_h^{n,*}\,\mathrm{d}\mathbf{x} = \int_{\partial K}\bar{\delta}\widehat{\nabla u_h^n}\cdot\mathbf{n}\bar{\delta} w_h^{n,*} - \bar{\delta}\widehat{u_h^n}\nabla\bar{\delta} w_h^{n,*}\cdot\mathbf{n}\,\mathrm{d}S. \tag{4.9}$$

For the resulting equations (4.6) and (4.9), by the same analysis that leads to the conservation of the semi-discrete mass (2.11) in Section 2.3, we can obtain

$$2\times\frac{1}{2h_t}\left[\sum_K\int_K \frac{|u_h^{n+1}| + |u_h^n|}{2} - \frac{|u_h^n| + |u_h^{n-1}|}{2}\,\mathrm{d}\mathbf{x}\right] = 0. \tag{4.10}$$

Thanks to (4.10) and (4.4), we have $M_h^{n+1} = M_h^n$ for all n. This finds that the fully discrete mass is conserved by using the fully discrete scheme (4.1)–(4.3).

For the fully discrete Hamiltonian conservation (4.5), we let the test function $\phi = \delta u_h^{n,*}$ in (4.1) to get

$$\int_K i\delta u_h^n \delta u_h^{n,*} + \bar{\delta} w_h^n \Delta\delta u_h^{n,*} + \bar{\delta} u_h^n \mathcal{G}\delta u_h^{n,*}\,\mathrm{d}\mathbf{x} = \int_{\partial K} -\bar{\delta}\widetilde{\nabla w_h^n}\delta u_h^{n,*} + \bar{\delta}\widetilde{w_h^n}\nabla\delta u_h^{n,*}\cdot\mathbf{n}\,\mathrm{d}S. \tag{4.11}$$

In (4.2) and (4.3), we choose the test function $\psi = \bar{\delta} w_h^{n,*}$ to obtain

$$\int_K w_h^{n+1} \bar{\delta} w_h^{n,*} - u_h^{n+1} \Delta \bar{\delta} w_h^{n,*} \,\mathrm{d}\mathbf{x} = \int_{\partial K} \widehat{\nabla u_h^{n+1}} \cdot \mathbf{n} \bar{\delta} w_h^{n,*} - \widehat{u_h^{n+1}} \nabla \bar{\delta} w_h^{n,*} \cdot \mathbf{n} \,\mathrm{d}S, \tag{4.12}$$

$$\int_K w_h^{n-1} \bar{\delta} w_h^{n,*} - u_h^{n-1} \Delta \bar{\delta} w_h^{n,*} \,\mathrm{d}\mathbf{x} = \int_{\partial K} \widehat{\nabla u_h^{n-1}} \cdot \mathbf{n} \bar{\delta} w_h^{n,*} - \widehat{u_h^{n-1}} \nabla \bar{\delta} w_h^{n,*} \cdot \mathbf{n} \,\mathrm{d}S. \tag{4.13}$$

Subtracting (4.12) from (4.13) and dividing the resulting equation by $2h_t$ yields

$$\int_K \delta w_h^n \bar{\delta} w_h^{n,*} - \delta u_h^n \Delta \bar{\delta} w_h^{n,*} \,\mathrm{d}\mathbf{x} = \int_{\partial K} \delta \widehat{\nabla u_h^n} \cdot \mathbf{n} \bar{\delta} w_h^{n,*} - \delta \widehat{u_h^n} \nabla \bar{\delta} w_h^{n,*} \cdot \mathbf{n} \,\mathrm{d}S. \tag{4.14}$$

For the resulting equations (4.11) and (4.14), using the same analysis for the conservation of the semi-discrete Hamiltonian (2.12) in Section 2.3, we find that

$$\sum_K \int_K \frac{|w_h^{n+1}| + |w_h^n|}{2} - \frac{|w_h^n| + |w_h^{n-1}|}{2} + \frac{F(|u_h^{n+1}|^2) + F\left(|u_h^n|^2\right)}{2} - \frac{F(|u_h^n|^2) + F(|u_h^{n-1}|^2)}{2} \,\mathrm{d}\mathbf{x} = 0.$$

This identity, in the light of (4.5), easily implies that $H_h^{n+1} = H_h^n$ for all n. Therefore, we prove that the fully discrete Hamiltonian is conserved using the fully discrete scheme (4.1)–(4.3). □

Note that the fully discrete scheme (4.1)–(4.3) can be rewritten into the following nonlinear algebraic equation

$$\mathbf{U}^{n+1} = \mathcal{L}\big(\mathbf{U}^{n-1}, \mathbf{U}^{n+1}\big) + \mathcal{N}\big(\mathbf{U}^{n-1}, \mathbf{U}^{n+1}\big),$$

where $\mathbf{U}$ contains the degrees of freedom for u_h, $\mathcal{L}$ and $\mathcal{N}$ are linear and nonlinear functions of $\mathbf{U}^{n-1}, \mathbf{U}^{n+1}$. For numerical implementations of the scheme, we will use Newton's method to find $\mathbf{U}^{n+1}$ for each time step t_{n+1}, and the stopping criteria is given such that both the absolute and relative differences between two successive updates are less than 10^{-8}. Since the second-order central difference is used in the time discretization and we are interested in the effect of the spatial discretization, we use the time step $h_t = 1 \times 10^{-4}$ to ensure that the error is dominated by the spatial discretization when using the Crank–Nicolson time integrator for the numerical experiments.

5. Numerical simulations

In this section, we present several numerical experiments to illustrate and support the convergence of the proposed DG scheme in Section 2. Throughout these studies, we use a standard modal basis formulation and the alternating flux (3.1) for simplicity of demonstration. In addition, the initial data are obtained by solving the problem (3.7) with scheme (3.8) and (3.9).

5.1. Linear problem in one-dimensional space

First, we consider the linear biharmonic Schrödinger equation

$$iu_t + u_{xxxx} = 0, \quad (x,t) \in (0, 4\pi) \times (0, 1], \tag{5.1}$$

with periodic boundary condition and initial condition $u(x,0) = \cos x + i \sin x$. Note that this linear problem has the following exact solution

$$u(x,t) = \cos(x+t) + i \sin(x+t).$$

We uniformly discretize the spatial interval through vertices $x_j = jh$, $j = 0, \cdots, N$, $h = 4\pi/N$. Throughout the studies, we present results by considering the degree of the approximation space for both u_h and w_h being $q \in \{1, 2, 3\}$.

TABLE 1. L^2/L^∞ errors and the corresponding convergence rates for u (the real part $\mathrm{Re}(u)$ and the imaginary part $\mathrm{Im}(u)$) for problem (5.1) using $\mathcal{P}^q$ polynomials for $q = 1, 2, 3$. The interval is divided into N uniform cells, and the terminal time is $T = 1$. These results show the optimal convergence is robust to the error norm.

q	N	Re(u)				Im(u)			
		L^2 error	Order	L^∞ error	Order	L^2 error	Order	L^∞ error	Order
1	10	1.00e−00	–	4.44e−01	–	1.00e−00	–	4.47e−01	–
	20	3.28e−01	1.61	1.45e−01	1.62	3.28e−01	1.61	1.47e−01	1.61
	40	8.78e−02	1.90	3.73e−02	1.96	8.78e−02	1.90	3.73e−02	1.98
	80	2.23e−02	1.97	9.18e−03	2.02	2.23e−02	1.97	9.18e−03	2.02
	160	5.61e−03	1.99	2.27e−03	2.01	5.61e−03	1.99	2.27e−03	2.01
2	10	6.74e−02	–	2.95e−02	–	6.74e−02	–	3.09e−02	–
	20	7.57e−03	3.16	3.72e−03	2.99	7.57e−03	3.16	3.90e−03	2.99
	40	9.24e−04	3.03	5.16e−04	2.85	9.24e−04	3.03	5.16e−04	2.92
	80	1.15e−04	3.01	6.73e−05	2.94	1.15e−04	3.01	6.73e−05	2.94
	160	1.43e−05	3.00	8.57e−06	2.97	1.43e−05	3.00	8.57e−06	2.97
3	10	4.06e−03	–	2.25e−03	–	4.06e−03	–	2.36e−03	–
	20	2.49e−04	4.03	1.44e−04	3.97	2.49e−04	4.03	1.37e−04	4.11
	40	1.55e−05	4.01	8.81e−06	4.03	1.55e−05	4.01	8.81e−06	3.96
	80	9.67e−07	4.00	5.54e−07	3.99	9.67e−07	4.00	5.54e−07	3.99
	160	6.06e−08	4.00	3.56e−08	3.96	6.06e-08	4.00	3.53e−08	3.97

Tables 1 and 2 show the L^2/L^∞ errors for the real and imaginary parts of u and w, respectively. Specifically, the L^2-error is evaluated by using the Gauss quadrature rule with $q+1$ Gauss nodes, and L^∞-error is evaluated by comparing the errors among Gauss quadrature nodes

$$\begin{aligned} \|\mathrm{Re}(u(x,1) - u_h(x,1))\|_{L^2(\Omega_h)} &= \left(\sum_K \sum_{j=0}^{q} \omega_j^K \big(u(x_j^K,1) - u_h(x_j^K,1)\big)^2 \right)^{1/2}, \\ \|\mathrm{Re}(u(x,1) - u_h(x,1))\|_{L^\infty(\Omega_h)} &= \max_{x\in\{x_j^K\}} |(u(x,1) - u_h(x,1))|, \end{aligned} \tag{5.2}$$

where x_j^K denotes the Gauss quadrature nodes in the element K and ω_j^K is the corresponding weight. Here we define only the real parts of the errors, while their imaginary parts can be measured similarly. We also include the corresponding numerical orders of accuracy subject to the variation of q and N. We find that the proposed scheme gives the robust and optimal $(q+1)$th order of accuracy across size N and error norms.

Figure 1 shows the numerical mass and Hamiltonian trajectories of the proposed ultraweak-local DG scheme for (5.1) with Crank–Nicolson time integrator. These approximations are obtained with degree $q = 2$ and spatial mesh size $N = 40$ up to the final time $T = 2000$. We note that the numerical mass and the Hamiltonian are conserved up to machine error.

Finally, Table 3 shows the L^2/L^∞ errors and the corresponding numerical orders of accuracy subject to the variation of q and N for the real and imaginary parts of u with the following inhomogeneous data

$$u(0,t) = \cos(t) + i\sin(t), \quad u(4\pi,t) = \cos(4\pi + t) + i\sin(4\pi + t). \tag{5.3}$$

In this case, we choose the numerical fluxes $\widetilde{\nabla w_h}$, $\widetilde{w_h}$, $\widehat{\nabla u_h}$ and $\widehat{u_h}$ at the physical boundaries as the exact data derived from (5.3). We find that the proposed scheme still gives the robust and optimal $(q+1)$th order

TABLE 2. L^2/L^∞ errors and the corresponding convergence rates for w (the real part $\mathrm{Re}(w)$ and the imaginary part $\mathrm{Im}(w)$) for problem (5.1) using $\mathcal{P}^q$ polynomials for $q = 1, 2, 3$. The interval is divided into N uniform cells; the terminal time is $T = 1$. All are chosen to be the same as those in Table 1.

q	N	Re(w)				Im(w)			
		L^2 error	Order	L^∞ error	Order	L^2 error	Order	L^∞ error	Order
	10	1.40e+00	–	5.64e−01	–	1.40e+00	–	5.48e−01	–
	20	3.19e−01	2.13	1.52e−01	1.89	3.19e−01	2.13	1.59e−01	1.79
1	40	9.10e−02	1.81	4.30e−02	1.82	9.10e−02	1.81	4.30e−02	1.89
	80	2.39e−02	1.93	1.11e−02	1.95	2.39e−02	1.93	1.11e−02	1.95
	160	6.08e−03	1.97	2.81e−03	1.99	6.08e−03	1.97	2.81e−03	1.99
	10	7.97e−02	–	5.10e−02	–	7.97e−02	–	5.30e−02	–
	20	7.58e−03	3.40	4.78e−03	3.41	7.58e−03	3.40	5.01e−03	3.40
2	40	9.24e−04	3.04	5.91e−04	3.02	9.24e−04	3.04	5.91e−04	3.08
	80	1.15e−04	3.01	7.22e−05	3.03	1.15e−04	3.01	7.22e−05	3.03
	160	1.43e−05	3.00	8.88e−06	3.02	1.43e−05	3.00	8.88e−06	3.02
	10	4.06e−03	–	2.49e−03	–	4.06e−03	–	2.47e−03	–
	20	2.49e−04	4.03	1.44e−04	4.11	2.49e−04	4.03	1.43e−04	4.11
3	40	1.55e−05	4.01	8.90e−06	4.02	1.55e−05	4.01	8.90e−06	4.01
	80	9.67e−07	4.00	5.55e−07	4.00	9.67e−07	4.00	5.55e−07	4.00
	160	6.06e−08	4.00	3.54e−08	3.97	6.06e−08	4.00	3.50e−08	3.99

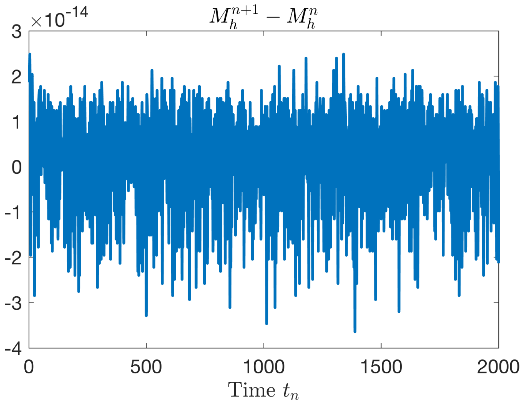

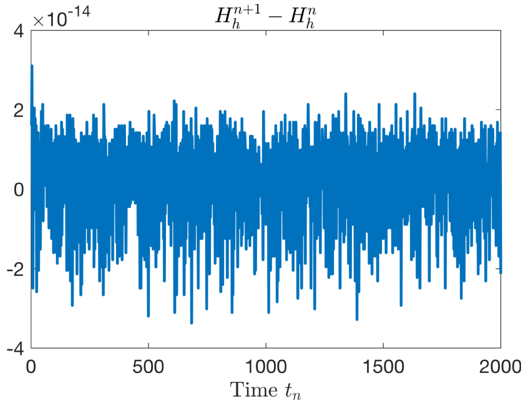

FIGURE 1. The *left* figure plots $M_h^{n+1} - M_h^n$ for problem (5.1) using the $\mathcal{P}^2$ polynomial on a uniform mesh of $N = 40$ up to a final time $T = 2000$, while the *right* figure plots $H_h^{n+1} - H_h^n$ under the same setting.

of accuracy over size N and error norms. We leave the theoretical analysis of the scheme (4.1)–(4.3) with inhomogeneous data for future study.

5.2. Defocusing nonlinear problem in one-dimensional space

We provide another set of studies on the theoretical convergence order of the proposed ultraweak-local DG scheme in studying the defocusing nonlinear biharmonic Schrödinger equation with $F'\left(|u|^2\right) = e^{|u|^2}$. We consider

TABLE 3. L^2/L^∞ errors and the corresponding convergence rates for u (the real part $\mathrm{Re}(u)$ and the imaginary part $\mathrm{Im}(u)$) for problem (5.1) with inhomogeneous data given in (5.3) using $\mathcal{P}^q$ polynomials for $q = 1, 2, 3$. The interval is divided into N uniform cells, and the terminal time is $T = 1$. These results show the optimal convergence is robust to the error norm.

q	N	Re(u)				Im(u)			
		L^2 error	Order	L^∞ error	Order	L^2 error	Order	L^∞ error	Order
1	10	1.26e−00	–	7.44e−01	–	1.50e−00	–	8.33e−01	–
	20	4.08e−01	1.63	2.39e−01	1.64	4.39e−01	1.77	2.29e−01	1.86
	40	7.04e−02	2.53	4.12e−02	2.54	1.17e−01	1.91	7.42e−02	1.63
	80	1.80e−02	1.97	1.14e−02	1.86	2.92e−02	2.00	1.83e−02	2.02
	160	4.44e−03	2.02	2.65e−03	2.10	7.26e−03	2.01	4.23e−03	2.11
2	10	1.02e−01	–	8.52e−02	–	9.01e−02	–	8.15e−02	–
	20	6.14e−03	4.05	5.15e−03	4.05	1.13e−02	3.00	8.23e−03	3.31
	40	6.80e−04	3.17	5.19e−04	3.31	8.76e−04	2.69	6.13e−04	3.75
	80	1.13e−04	2.57	7.21e−05	2.85	1.13e−04	2.96	7.43e−05	3.04
	160	1.43e−05	2.98	8.98e−06	3.01	1.43e−05	2.98	9.01e−06	3.04
3	10	5.02e−03	–	4.20e−03	–	5.78e−03	–	3.99e−03	–
	20	3.44e−04	3.87	2.86e−04	3.87	2.24e−04	4.69	1.35e−04	4.88
	40	1.58e−05	4.44	9.31e−06	4.94	1.55e−05	3.85	9.14e−06	3.89
	80	9.74e−07	4.02	5.64e−07	4.05	9.72e−07	4.00	5.59e−07	4.03
	160	6.07e−08	4.00	3.59e−08	3.97	6.12e−08	3.99	3.50e−08	4.00

$$iu_t + u_{xxxx} + ue^{|u|^2} = f(x,t), \quad (x,t) \in (0,4\pi) \times (0,1], \tag{5.4}$$

with periodic boundary conditions. Note that such a nonlinear term is chosen so that we can demonstrate the computational efficiency and robustness of the proposed scheme to strong nonlinearity without discussing many of the real physical applications here. In particular, given by a properly chosen external forcing $f(x,t)$, this problem has an analytical solution of the following explicit form

$$u(x,t) = \cos(x+t) + i\sin(x+t).$$

Choosing the degree of approximation $q = 2$ and the number of cells $N = 80$, we present in Figure 2 the snapshots of the numerical solution u_h and w_h at $t = 1000$. These simulations also provide visual evidence that our numerical solutions agree very well with the exact solution.

We use the same spatial discretization as in Section 5.1 and show in Tables 4 and 5 the L^2/L^∞ errors for the real and imaginary parts of both u and w. We observe results similar to those for the linear biharmonic Schrödinger equations in Section 5.1. In particular, we find optimal $q+1$ convergence for both the real and imaginary parts of u and w.

5.3. Focusing nonlinear problem in one-dimensional space

We now provide another set of experiments by considering nonlinear biharmonic Schrödinger equations with an indefinite Hamiltonian. Specifically, we test the problem

$$iu_t = -u_{xxxx} - uF'\big(|u|^2\big), \quad x \in (0,4\pi), \quad t \in (0,100]$$

under two types of nonlinearity

$$(a).\ F'\big(|u|^2\big) = -|u|^2, \quad (b).\ F'(|u|^2) = -|u|^4.$$

TABLE 4. L^2/L^∞ errors and the corresponding convergence rates for u of problem (5.4) using $\mathcal{P}^q$ polynomials for $q = 1, 2, 3$ on a uniform mesh of N cells up to terminal time $T = 1$. This table adds additional evidence that supports the optimal and robust convergence of the proposed scheme.

q	N	Re(u)				Im(u)			
		L^2 error	Order	L^∞ error	Order	L^2 error	Order	L^∞ error	Order
1	10	5.30e−01	–	2.10e−01	–	5.30e−01	–	2.18e−01	–
	20	1.45e−01	1.88	5.72e−02	1.87	1.45e−01	1.88	5.75e−02	1.92
	40	3.96e−02	1.87	1.76e−02	1.70	3.96e−02	1.87	1.76e−02	1.71
	80	1.02e−02	1.96	4.72e−03	1.90	1.02e−02	1.96	4.72e−03	1.90
	160	2.56e−03	1.99	1.21e−03	1.97	2.56e−03	1.99	1.21e−03	1.97
2	10	5.79e−02	–	3.69e−02	–	5.79e−02	–	3.57e−02	–
	20	7.39e−03	2.97	4.47e−03	3.05	7.39e−03	2.97	4.66e−03	2.94
	40	9.18e−04	3.01	5.65e−04	2.98	9.18e−04	3.01	5.65e−04	3.04
	80	1.15e−04	3.00	7.04e−05	3.01	1.15e−04	3.00	7.04e−05	3.01
	160	1.43e−05	3.00	8.76e−06	3.01	1.43e−05	3.00	8.76e−06	3.01
3	10	3.98e−03	–	2.31e−03	–	3.98e−03	–	2.37e−03	–
	20	2.49e−04	4.00	1.44e−04	4.01	2.49e−04	4.00	1.38e−04	4.11
	40	1.55e−05	4.00	8.81e−06	4.03	1.55e−05	4.00	8.81e−06	3.97
	80	9.67e−07	4.00	5.54e−07	3.99	9.67e−07	4.00	5.54e−07	3.99
	160	6.05e−08	4.00	3.52e−08	3.97	6.05e−08	4.00	3.49e−08	3.99

TABLE 5. L^2/L^∞ errors and the corresponding convergence rates for w of problem (5.4) using $\mathcal{P}^q$ polynomials for $q = 1, 2, 3$ on a uniform mesh of N cells up to terminal time $T = 1$.

q	N	Re(w)				Im(w)			
		L^2 error	Order	L^∞ error	Order	L^2 error	Order	L^∞ error	Order
1	10	9.52e−01	–	4.09e−01	–	9.52e−00	–	3.94e−01	–
	20	1.90e−01	2.33	9.52e−02	2.10	1.90e−01	2.32	9.06e−02	2.12
	40	5.07e−02	1.90	2.64e−02	1.84	5.07e−02	1.90	2.64e−02	1.78
	80	1.28e−02	1.99	6.80e−03	1.96	1.28e−02	1.99	6.80e−02	1.96
	160	3.18e−03	2.01	1.72e−03	1.99	3.18e−03	2.01	1.72e−03	1.99
2	10	4.17e−02	–	1.73e−02	–	4.17e−02	–	1.74e−02	–
	20	6.98e−03	2.58	3.82e−03	2.18	6.98e−03	2.58	3.91e−03	2.16
	40	9.06e−04	2.94	5.35e−04	2.84	9.06e−04	2.94	5.35e−04	2.87
	80	1.14e−04	3.00	6.89e−05	2.96	1.14e−04	3.00	6.89e−05	2.96
	160	1.43e−05	3.00	8.68e−06	2.99	1.43e−05	3.00	8.68e−06	2.99
3	10	3.05e−03	–	1.47e−03	–	3.05e−03	–	1.51e−03	–
	20	2.29e−04	3.73	1.24e−04	3.57	2.29e−04	3.73	1.23e−04	3.61
	40	1.52e−05	3.92	8.57e−06	3.85	1.52e−05	3.92	8.57e−06	3.84
	80	9.62e−07	3.98	5.49e−07	3.96	9.62e−07	3.98	5.49e−07	3.96
	160	6.04e−08	3.99	3.48e−08	3.98	6.03e−08	3.99	3.48e−08	3.98

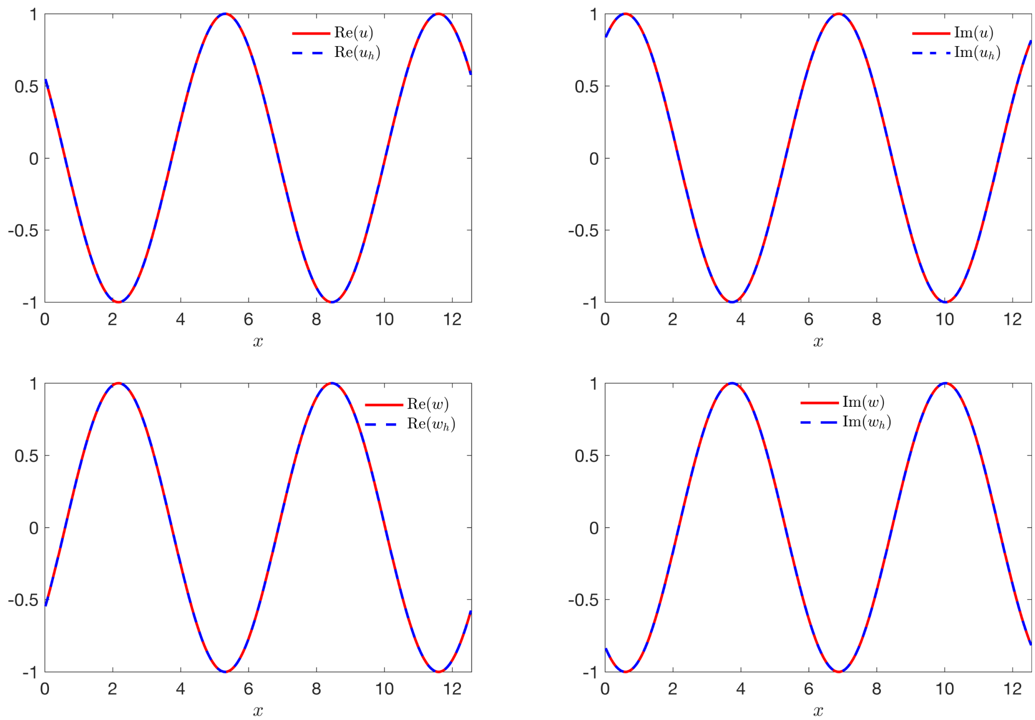

FIGURE 2. Snapshots of the numerical and exact solutions of problem (5.4) at $T = 100$, where the numerical solution is obtained using the $\mathcal{P}^2$ polynomial on a uniform mesh of $N = 80$. These plots provide clear support for the proposed scheme to approximate the exact solution, even up to a significantly long time.

Again, we study these problems with the same periodic boundary conditions and the following initial data as in Section 5.2

$$u(x, 0) = \cos x + i \sin x.$$

We note that no explicit solution is available for this focusing problem.

Finally, we use the same spatial discretization as in Section 5.1 with the approximation order $q = 2$ and the number of cells $N = 80$. Figure 3 shows the time dynamics of the discrete solution u_h under these different nonlinear media up to $T = 100$. From top to bottom we choose $F'(u) = -|u|^2$ and $F'(u) = -|u|^4$, respectively. On the top panel, we see that u_h is still stable up to $t \approx 30$, but then its dynamics rotate and a stable time-periodic profile develops. On the bottom panel, we see that a new stable time-periodic profile evolves from the original solution around $t \approx 13$.

5.4. Defocusing nonlinear problem in two-dimensional space

In this example we study the convergence of the ultraweak-local DG scheme for the nonlinear Schrödinger equation with $F'(|u|^2) = |u|^2$ in two space dimensions. Specifically, we solve

$$iu_t + \Delta^2 u + u|u|^2 = 0, \quad (x, y, t) \in (0, 2\pi) \times (0, 2\pi) \times (0, 1], \tag{5.5}$$

with periodic boundary conditions and initial data

$$u(x, y, 0) = \cos(x + y) + i \sin(x + y).$$

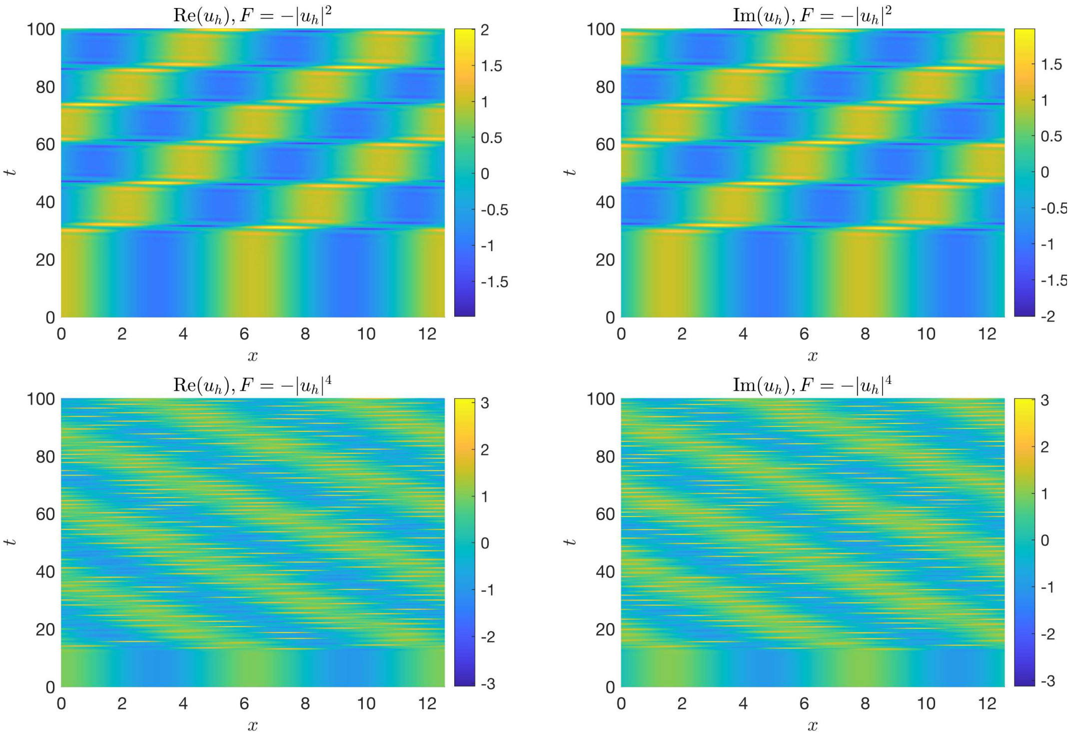

FIGURE 3. Spatiotemporal dynamics of numerical solutions with the nonlinearity of the medium $F'(|u_h|^2) = -|u_h|^2$ on the top and $F'(|u_h|) = -|u_h|^4$ on the bottom. It is easy to see from these plots that the spatiotemporal dynamics of the problem depend heavily on the choice of medium and are extremely complex, including oscillations. *Top*: the real part of u_h (*left*) and the imaginary part of u_h (*right*) with $F'(|u_h|^2) = -|u_h|^2$. *Bottom*: the real part of u_h (*left*) and the imaginary part of u_h (*right*) with $F'(|u_h|^2) = -|u_h|^4$.

This yields the following exact solution

$$u(x, y, t) = \cos(x + y + 5t) + i \sin(x + y + 5t).$$

The discretization is performed with elements over the Cartesian lattices formed by $(x_k, y_j) = (kh, jh), k, j = 0, 1, ..., N$ with $h = 2\pi/N$. Here we present only the results for u, since the results for both u and w are similar to the one-dimensional problems. Table 6 shows the L^2/L^∞ errors for the real and imaginary parts of u, where we observe optimal convergence for both parts in both norms.

5.5. Mixed boundary condition in two-dimensional space

Our final example considers the nonlinear biharmonical Schrödinger equation in 2D.

$$iu_t + \Delta^2 u + u(2 + \sin(|u|^2)) = f(x, y, t), \quad (x, y, t) \in (0, 1) \times (0, 1) \times (0, 1], \tag{5.6}$$

with the following mixed boundary conditions:

$$\texttt{top boundary:}\begin{cases} u(x, 2\pi, t) = 0, \\ u_y(x, 2\pi, t) = 0, \end{cases} \qquad \texttt{bottom boundary:}\begin{cases} u_{yy}(x, 0, t) = 0, \\ u_{yyy}(x, 0, t) = 0, \end{cases}$$

TABLE 6. L^2/L^∞ errors and the corresponding convergence rates for u of problem (5.5) using $\mathcal{Q}^q$ polynomials, $q = 1, 2, 3$. We choose a uniform Cartesian mesh of $N \times N$ elements and the terminal time $T = 1$.

q	$N \times N$	Re(u)				Im(u)			
		L^2 error	Order	L^∞ error	Order	L^2 error	Order	L^∞ error	Order
1	4×4	7.40e−00	–	2.17e−00	–	7.40e−00	–	2.17e−00	–
	8×8	3.28e−00	1.17	8.34e−01	1.38	3.28e−00	1.17	8.34e−01	1.38
	16×16	9.05e−01	1.86	2.16e−01	1.95	9.05e−01	1.86	2.16e−01	1.95
	32×32	2.30e−01	1.98	5.38e−02	2.00	2.30e−01	1.98	5.38e−02	2.00
2	4×4	6.25e−01	–	1.98e−01	–	6.25e−01	–	1.98e−01	–
	8×8	4.78e−02	3.71	1.67e−02	3.58	4.78e−02	3.71	1.67e−02	3.57
	16×16	4.91e−03	3.28	1.79e−03	3.23	4.91e−03	3.28	1.79e−03	3.23
	32×32	6.12e−04	3.01	2.22e−04	3.01	6.12e−04	3.01	2.22e−04	3.01
3	4×4	2.73e−02	–	1.09e−02	–	2.73e−02	–	1.09e−02	–
	8×8	1.55e−03	4.14	7.05e−04	3.95	1.55e−03	4.14	7.05e−04	3.95
	16×16	9.54e−05	4.02	4.42e−05	3.99	9.54e−05	4.02	4.42e−05	3.99
	32×32	5.93e−06	4.01	2.73e−06	4.02	5.93e−06	4.01	2.73e−06	4.02

$$\texttt{left boundary:}\begin{cases} u_{xx}(0,y,t) = u_{xx}(1,y,t), \\ u_{xxx}(0,y,t) = u_{xxx}(1,y,t), \end{cases} \quad \texttt{right boundary:}\begin{cases} u(1,y,t) = u(0,y,t), \\ u_x(1,y,t) = u_x(0,y,t). \end{cases}$$

Then the exact solution of (5.6) is

$$u(x,y,t) = (\cos 2\pi x + i \sin 2\pi x) y^4 (y-1)^4 e^t.$$

Table 7 shows the L^2/L^∞ errors of u for problem (5.6), while Table 8 shows the L^2/L^∞ errors of w. Here, both errors are computed as in (5.2) by considering all quadrature nodes in the 2D computational domain. We observe optimal convergence for both u and w when $q = 2, 3$. When $q = 1$, we observe a super-convergence $q+2$ for u in both L^2/L^∞; optimal convergence for w in L^2, and a super-convergence $q+2$ in L^∞.

6. Brief discussion

In conclusion, we have developed and analyzed an ultraweak-local DG method for nonlinear biharmonic Schrödinger equations. We extend the local DG scheme by introducing a second-order spatial derivative as an auxiliary variable. This maneuver reduces the memory required for the variables to be solved, as well as the number of equations to be solved at each single time step, compared to the local DG scheme applied directly to the problem (2.1). The scheme is also stable without the use of a penalty term. We have proved and demonstrated the stability of the scheme for the special projection operators; moreover, we also obtain optimal L^2 error estimates under these settings. We further show that the fully discrete scheme combined with the Crank–Nicolson time integrator is conservative. Our numerical experiments demonstrate the theoretical results and reveal the rich and complex spatiotemporal dynamics of these linear/nonlinear problems. Our work also suggests several directions for the future development of the proposed scheme. The problems of nonlocal nonlinearity, which capture physical phenomena not described by the local operators, deserve academic attention. Moreover, one can also try to obtain the error estimates for more general numerical fluxes. In addition, our approach can be easily extended to two-dimensional unstructured triangular meshes. However, the derivation of optimal error estimates will require more work and we leave this to future work.

TABLE 7. L^2/L^∞ errors and the corresponding convergence rates for u of problem (5.6) using $\mathcal{Q}^q$ polynomials polynomials, $q = 1, 2, 3$. We choose a uniform Cartesian mesh of $N \times N$ elements and the terminal time $T = 1$.

q	$N \times N$	Re(u)				Im(u)			
		L^2 error	Order	L^∞ error	Order	L^2 error	Order	L^∞ error	Order
1	15×15	1.78e−02	–	8.47e−02	–	1.78e−02	–	8.47e−02	–
	20×20	7.33e−03	3.09	3.50e−02	3.07	7.33e−03	3.09	3.50e−02	3.06
	25×25	3.67e−03	3.10	1.77e−02	3.06	3.67e−03	3.10	1.77e−02	3.07
	30×30	2.08e−03	3.11	1.01e−02	3.08	2.08e−03	3.11	1.01e−02	3.08
	35×35	1.29e−03	3.10	6.27e−03	3.09	1.29e−03	3.10	6.27e−03	3.09
2	15×15	3.29e−04	–	2.85e−03	–	3.29e−04	–	2.85e−03	–
	20×20	1.17e−04	3.60	1.04e−03	3.50	1.17e−04	3.60	1.04e−03	3.50
	25×25	5.18e−05	3.65	5.12e−04	3.18	5.18e−05	3.65	5.11e−04	3.18
	30×30	2.64e−05	3.69	2.94e−04	3.04	2.64e−05	3.69	2.93e−04	3.06
	35×35	1.50e−05	3.67	1.85e−04	3.00	1.50e−05	3.67	1.85e−04	2.98
3	15×15	8.88e−06	–	1.86e−04	–	8.88e−06	–	1.87e−04	–
	20×20	2.59e−06	4.29	6.38e−05	3.73	2.59e−06	4.29	6.38e−05	3.74
	25×25	9.83e−07	4.34	2.73e−05	3.81	9.83e−07	4.34	2.73e−05	3.81
	30×30	4.43e−07	4.37	1.35e−05	3.86	4.43e−07	4.37	1.35e−05	3.86
	35×35	2.25e−07	4.39	7.42e−06	3.88	2.25e−07	4.39	7.42e−06	3.88

TABLE 8. L^2/L^∞ errors and the corresponding convergence rates for w of problem (5.6) using $\mathcal{Q}^q$ polynomials, $q = 1, 2, 3$. We choose a uniform Cartesian mesh of $N \times N$ elements and the terminal time $T = 1$.

q	$N \times N$	Re(w)				Im(w)			
		L^2 error	Order	L^∞ error	Order	L^2 error	Order	L^∞ error	Order
1	15×15	7.10e−03	–	3.22e−02	–	7.10e−03	–	3.20e−02	–
	20×20	2.94e−03	3.07	1.26e−02	3.27	2.94e−03	3.07	1.26e−02	3.26
	25×25	1.56e−03	2.83	6.24e−03	3.13	1.56e−03	2.83	6.23e−03	3.14
	30×30	9.61e−04	2.66	3.56e−03	3.09	9.61e−04	2.66	3.55e−03	3.08
	35×35	6.51e−04	2.53	2.23e−03	3.03	6.51e−04	2.53	2.23e−03	3.02
2	15×15	1.76e−04	–	7.67e−04	–	1.76e−04	–	7.67e−04	–
	20×20	7.49e−05	2.96	4.16e−04	2.13	7.49e−05	2.96	4.16e−04	2.13
	25×25	3.57e−05	3.33	1.67e−04	4.10	3.57e−05	3.33	1.66e−04	4.11
	30×30	2.04e−05	3.08	9.99e−05	2.81	2.04e−05	3.08	9.99e−05	2.80
	35×35	1.27e−05	3.06	6.45e−05	2.84	1.27e−05	3.06	6.45e−05	2.84
3	15×15	5.92e−06	–	2.28e−05	–	5.92e−06	–	2.27e−05	–
	20×20	1.88e−06	4.00	7.15e−06	4.03	1.88e−06	4.00	7.15e−06	4.02
	25×25	7.69e−07	4.00	2.91e−06	4.02	7.69e−07	4.00	2.91e−06	4.03
	30×30	3.71e−07	4.00	1.40e−06	4.02	3.71e−07	4.00	1.40e−06	4.03
	35×35	2.00e−07	4.01	7.55e−07	4.01	2.00e−07	4.01	7.54e−07	4.01

Acknowledgements

The authors would like to thank the reviewers and the editor for their valuable comments and constructive suggestions, which significantly improved our work.

Funding

QW is partially supported by Guanghua Talent Project of SWUFE.

References

[1] G.P. Agrawal, Nonlinear fiber optics, in Nonlinear Science at the Dawn of the 21st Century. Springer, Heidelberg (2000) 195–211.

[2] G.D. Akrivis, Finite difference discretization of the cubic Schrödinger equation. *IMA J. Numer. Anal.* **13** (1993) 115–124.

[3] G.D. Akrivis, V.A. Dougalis and O.A. Karakashian, On fully discrete Galerkin methods of second-order temporal accuracy for the nonlinear Schrödinger equation. *Numer. Math.* **59** (1991) 31–53.

[4] I. Babuška, The finite element method with penalty. *Math. Comput.* **27** (1973) 221–228.

[5] I. Babuška and M. Zlámal, Nonconforming elements in the finite element method with penalty. *SIAM J. Numer. Anal.* **10** (1973) 863–875.

[6] G.A. Baker, Finite element methods for elliptic equations using nonconforming elements. *Math. Comput.* **31** (1977) 45–59.

[7] W. Bao and Y. Cai, Optimal error estimates of finite difference methods for the Gross–Pitaevskii equation with angular momentum rotation. *Math. Comput.* **82** (2013) 99–128.

[8] W. Bao, D. Jaksch and P.A. Markowich, Numerical solution of the Gross–Pitaevskii equation for Bose–Einstein condensation. *J. Comput. Phys.* **187** (2003) 318–342.

[9] G. Baruch and G. Fibich, Singular solutions of the L^2-supercritical biharmonic nonlinear Schrödinger equation. *Nonlinearity* **24** (2011) 1843.

[10] G. Baruch, G. Fibich and E. Mandelbaum, Ring-type singular solutions of the biharmonic nonlinear Schrödinger equation. *Nonlinearity* **23** (2010) 2867.

[11] G. Baruch, G. Fibich and E. Mandelbaum, Singular solutions of the biharmonic nonlinear Schrödinger equation. *SIAM J. Appl. Math.* **70** (2010) 3319–3341.

[12] C. Besse, A relaxation scheme for the nonlinear Schrödinger equation. *SIAM J. Numer. Anal.* **42** (2004) 934–952.

[13] J. Bona, H. Chen, O. Karakashian and Y. Xing, Conservative, discontinuous Galerkin–methods for the generalized Korteweg–de Vries equation. *Math. Comput.* **82** (2013) 1401–1432.

[14] O. Cessenat and B. Despres, Application of an ultra weak variational formulation of elliptic PDEs to the two-dimensional Helmholtz problem. *SIAM J. Numer. Anal.* **35** (1998) 255–299.

[15] Q. Chang, B. Guo and H. Jiang, Finite difference method for generalized Zakharov equations. *Math. Comput.* **64** (1995) 537–553.

[16] A. Chen, F. Li and Y. Cheng, An ultra-weak discontinuous Galerkin method for Schrödinger equation in one dimension. *J. Sci. Comput.* **78** (2019) 772–815.

[17] Y. Cheng and C.-W. Shu, A discontinuous Galerkin finite element method for time dependent partial differential equations with higher order derivatives. *Math. Comput.* **77** (2008) 699–730.

[18] P.G. Ciarlet, The finite element method for elliptic problems. *Class. Appl. Math.* **40** (2002) 1–511.

[19] B. Cockburn and C.-W. Shu, The local discontinuous Galerkin method for time-dependent convection-diffusion systems. *SIAM J. Numer. Anal.* **35** (1998) 2440–2463.

[20] B. Cockburn and C.-W. Shu, Foreword for the special issue on discontinuous Galerkin method. *J. Sci. Comput.* **22** (2005) 1–3.

[21] B. Cockburn, G. Kanschat, I. Perugia and D. Schötzau, Superconvergence of the local discontinuous Galerkin method for elliptic problems on Cartesian grids. *SIAM J. Numer. Anal.* **39** (2001) 264–285.

[22] S. Cui and C. Guo, Well-posedness of higher-order nonlinear Schrödinger equations in Sobolev spaces $H^s(\mathbb{R}^n)$ and applications. *Nonlinear Anal.* **67** (2007) 687–707.

[23] I. Dag, A quadratic B-spline finite element method for solving nonlinear Schrödinger equation. *Comput. Methods Appl. Mech. Eng.* **174** (1999) 247–258.

[24] C. Dawson, Foreword for the special issue on discontinuous Galerkin method. *Comput. Methods Appl. Mech. Eng.* **195** (2006) 8–68.

[25] B. Despres, Sur une formulation variationnelle de type ultra-faible. *C. R. Acad. Sci. Paris Sér. I Math.* **318** (1994) 939–944.

[26] B. Dong and C.-W. Shu, Analysis of a local discontinuous Galerkin method for linear time-dependent fourth-order problems. *SIAM J. Numer. Anal.* **47** (2009) 3240–3268.

[27] B. Ilan, G. Fibich and G. Papanicolaou, Self-focusing with fourth-order dispersion. *SIAM J. Appl. Math.* **62** (2002) 1437–1462.

[28] O. Karakashian and C. Makridakis, A space-time finite element method for the nonlinear Schrödinger equation: the continuous Galerkin method. *SIAM J. Numer. Anal.* **36** (1999) 1779–1807.

[29] V. Karpman, Stabilization of soliton instabilities by higher-order dispersion: fourth-order nonlinear Schrödinger-type equations. *Phys. Rev. E* **53** (1996) R1336.

[30] V. Karpman and A. Shagalov, Stability of solitons described by nonlinear Schrödinger-type equations with higher-order dispersion. *Phys. D* **144** (2000) 194–210.

[31] J. Li, D. Zhang, X. Meng and B. Wu, Analysis of local discontinuous Galerkin methods with generalized numerical fluxes for linearized KdV equations. *Math. Comput.* **89** (2020) 2085–2111.

[32] D. Pathria and J.L. Morris, Pseudo-spectral solution of nonlinear Schrödinger equations. *J. Comput. Phys.* **87** (1990) 108–125.

[33] B. Pausader, The cubic fourth-order Schrödinger equation. *J. Funct. Anal.* **256** (2009) 2473–2517.

[34] W.H. Reed and T.R. Hill, Triangular mesh methods for the neutron transport equation. Technical report, Los Alamos Scientific Laboratory, New Mexico, United States of America (1973).

[35] M. Robinson, G. Fairweather and B. Herbst, On the numerical solution of the cubic Schrödinger equation in one space variable. *J. Comput. Phys.* **104** (1993) 277–284.

[36] C.-W. Shu, Discontinuous Galerkin methods for time-dependent convection dominated problems: basics, recent developments and comparison with other methods, in Building Bridges: Connections and Challenges in Modern Approaches to Numerical Partial Differential Equations. Springer, Cham (2016) 371–399.

[37] Q. Tao, Y. Xu and C.-W. Shu, An ultraweak-local discontinuous Galerkin method for PDEs with high order spatial derivatives. *Math. Comput.* **89** (2020) 2753–2783.

[38] Q. Tao, Y. Xu and C.-W. Shu, A discontinuous Galerkin method and its error estimate for nonlinear fourth-order wave equations. *J. Comput. Appl. Math.* **386** (2021) 113230.

[39] M.F. Wheeler, An elliptic collocation-finite element method with interior penalties. *SIAM J. Numer. Anal.* **15** (1978) 152–161.

[40] A. Xiao, C. Wang and J. Wang, Conservative linearly-implicit difference scheme for a class of modified Zakharov systems with high-order space fractional quantum correction. *Appl. Numer. Math.* **146** (2019) 379–399.

[41] Y. Xu and C.-W. Shu, Optimal error estimates of the semidiscrete local discontinuous Galerkin methods for high order wave equations. *SIAM J. Numer. Anal.* **50** (2012) 79–104.

[42] J. Yan and C.-W. Shu, A local discontinuous Galerkin method for KdV type equations. *SIAM J. Numer. Anal.* **40** (2002) 769–791.

[43] N. Yi, Y. Huang and H. Liu, A conservative discontinuous Galerkin method for nonlinear electromagnetic Schrödinger equations. *SIAM J. Sci. Comput.* **41** (2019) B1389–B1411.

[44] L. Zhang, A local energy-based discontinuous Galerkin method for fourth-order semilinear wave equations. *IMA J. Numer. Anal.* (2023). DOI: 10.1093/imanum/drad076.

[45] G. Zhang and C. Su, A conservative linearly-implicit compact difference scheme for the quantum Zakharov system. *J. Sci. Comput.* **87** (2021) 1–24.

[46] H. Zhang, B. Wu and X. Meng, A local discontinuous Galerkin method with generalized alternating fluxes for 2D nonlinear Schrödinger equations. *Commun. Appl. Math. Comput.* **1** (2022) 84–107.

Please help to maintain this journal in open access!

This journal is currently published in open access under the Subscribe to Open model (S2O). We are thankful to our subscribers and supporters for making it possible to publish this journal in open access in the current year, free of charge for authors and readers.

Check with your library that it subscribes to the journal, or consider making a personal donation to the S2O programme by contacting subscribers@edpsciences.org.

More information, including a list of supporters and financial transparency reports, is available at https://edpsciences.org/en/subscribe-to-open-s2o.